This document was prepared for the ETI by third parties under contract to the ETI. The ETI is making these documents and data available to the public to inform the debate on low carbon energy innovation and deployment.

Programme Area: Marine

Project: PerAWAT

Title: Report on Characterisation and Assessment of the Availability of Resource at Example UK Sites

Abstract:

This report provides a characterisation and assessment of the availability of tidal resource at example sitees across the UK.

Context:

The Performance Assessment of Wave and Tidal Array Systems (PerAWaT) project, launched in October 2009 with £8m of ETI investment. The project delivered validated, commercial software tools capable of significantly reducing the levels of uncertainty associated with predicting the energy yield of major wave and tidal stream energy arrays. It also produced information that will help reduce commercial risk of future large scale wave and tidal array developments.

Energy Technologies Institute

PerAWaT

WG3 WP6 D7 — REPORT ON CHARACTERISATION AND ASSESSMENT OF THE AVAILABILITY OF RESOURCE AT EXAMPLE UK SITES

Authors S. Serhadlioglu, T.A.A. Adcock,
G.T. Houlsby, and A.G.L. Borthwick

Version 1.0

Date 14/08/2013

Revision History		
Issue / Version	Issue Date	Summary
0.0	31/07/2013	Submitted to GH
1.0	14/08/2013	Amended version of the report submitted to GH

Executive Summary

WG3 WP6 D7 aims to present an assessment of the resource availability for each UK sites. The present report gives a clear description of the simulations undertaken within the assessment and evaluates the maximum available power at each site for different array configurations. The hydrodynamic effects of including the fundamental device concept (FDC) tidal arrays are presented considering the changes in the local velocity field by considering the M_2 tidal constituent. The effect of tidal arrays in the computational domain is modelled as a line sink of momentum using Linear Momentum Actuator Disk Theory (LMADT).

CONTENTS

1. Introduction

Acceptance Criteria

Table 1 lists the acceptance criteria for the present deliverable. The report gives a detailed description of the simulations undertaken to estimate the maximum available power for different array configurations at each site of interest. The analysis is extended to show the change in the local flow field by considering the M_2 tide, which is representative of an average tidal cycle occurring in the UK waters (Uncles, 1983). It is not intended in this work package to evaluate the optimum array configurations to generate the maximum power at each site. This work package mainly focuses on developing and applying an elaborate numerical scheme for predicting maximum power that is available to arrays of turbines, modelled as momentum sinks using Linear Momentum Actuator Disk Theory (Houlsby *et al.*, 2008).

Table 1 Acceptance criteria

Deliverable	Acceptance criteria	Location in report
WG3 WP6 D7: Report on characterization and assessment of the availability of resource at example UK sites.	Report gives clear description of the numerical simulations for each UK site (methodology), and the hydrodynamic effects of tidal energy extraction that result from including various FDC tidal array characterizations developed elsewhere in WG3. Report includes a classification of tidal sites relative to generic coastal basins – i.e. availability of resource at different sites.	Anglesey Skerries: a. Methodology: pp. 13-25 b. Hydrodynamic Effects: pp. 25-30 Bristol Channel: a. Methodology: pp. 30-45 b. Hydrodynamic Effects: pp. 45-48 Pentland Firth: a. Methodology: pp. 48-54 b. Hydrodynamic Effects: pp. 54-56

Resource Assessment

Tidal power obtained from turbines offers potentially large renewable power supply to the UK. With this in mind, Draper (2011) considered various idealised coastline geometries, which can induce fast tidal flows and so are of interest in placing tidal turbines. In WG3 WP6, the aim is to examine the power potential for certain candidates including a headland (Anglesey), a strait (Pentland Firth) and a resonant bay (Bristol Channel).

Various approaches have been taken to assess the tidal resources. The first is based on the undisturbed kinetic energy flux (Black and Veatch, 2005). This approach provides an incorrect estimate of the resources, as there is no direct proportionality between the kinetic energy flux and available power (Draper *et al.*, 2011). A second approach involves numerical modelling of the sites using two-dimensional shallow water solvers. In this approach, the far-field effects of the turbine array deployment are represented by means of an additional bed roughness coefficient in the governing equations (*i.e.* Blunden and Bahaj, 2006). An alternative to this approach is presented by Draper *et al.* (2011), in which the turbine arrays are described using a near-field approximation that is embedded in a two-dimensional discontinuous Galerkin shallow water model. The near-field approach enables a distinction to be made between the available power and the total power extracted from the site. Assuming that the tidal devices are evenly spaced and the length of the downstream mixing zone is sufficiently smaller than the mesh discretisation, Draper (2011) demonstrated that the effects of tidal arrays could be represented using a line sink of momentum. This approach is used in this work.

The implementation of momentum sink into the DG-ADCIRC numerical code has been described in WG3 WP6 D5. The present report considers application of the altered numerical code to the sites of interest. The results are presented focusing on the maximum available power, maximum extracted power from the stream, and the hydrodynamic effects of such power extraction from the designated sites.

Limitations of Shallow Water Models

For many years, the two-dimensional shallow water equations have been successfully employed to model tidal hydrodynamics. Recently, shallow water models have been used to estimate the total power that can be extracted from the tidal stream in the areas of interest. Vogel *et al.* (2013a) emphasise that estimation of the maximum available power to the turbine arrays is dependent on accurately modelling the mass flux and velocity variations in the flow that passes through the turbines. In the literature, an enhanced resistance to the flow is commonly introduced in the governing equations in order to represent the tidal devices. This approach is found to be inadequate in evaluating the power potential of a site as it overestimates the power extracted from the flow field due to the incorrect velocity variations across the turbines (Vogel *et al.,* 2013a; Draper, 2011).

Analytical modelling is a good way of predicting the velocity at the turbines as well as the velocity change across the turbines. Houlsby *et al.* (2008) has used Linear Momentum Actuator Disk Theory that is applied to an open-channel flow to investigate the flow conditions where the turbines are placed across the width of an idealised channel. This approach is then improved in order to investigate the flow behaviour when the turbines are only partially blocking the channel (Nishino and Willden, 2012; Vogel *et al.,* 2013b). The studies show that there are two fundamental scales of the flow that require attention. The first involves the turbine scale flow where the focus is on an individual tidal device and the immediate wake downstream of the turbine. Three-dimensional models are employed in order to model the flow passing through a turbine that ensures the necessary grid resolution in order to calculate the power available to the turbine and the total power extracted from the flow, which includes the mixing losses in the wake. The second is the array scale flow, which basically considers the wake of a turbine array and the flow passing around the array in a site. Our model focuses on the array scale flow, in which the individual array characteristics are declared using a relevant wake velocity coefficient and a blockage ratio supplied with the upstream flow conditions as described in Draper (2011). The results presented in this report are achieved by using LMADT to represent the turbines to calculate the associated momentum removal from the flow. Application of LMADT in a discontinuous Galerkin solver enables us to make a

distinction between the power available to the turbines and the total power extracted from the stream. The model presented in the present report is capable of modelling the fundamental physics involved in a basin scale flow field. Representing the flow conditions of a turbine scale flow is not within the capacity of our model, as the resolution involved in that scale is significantly smaller than resolution of the model that considers large areas around the UK.

Another limitation of the model presented here is due to the nature of the shallow water equations. In the shallow water models, the flow is considered nearly horizontal thus the vertical velocity component is negligible when compared to the horizontal velocity components (Falconer, 1993). The associated vertical velocity profile is then introduced by including the bed friction coefficient in the governing equations. Stansby and Lloyd (2001) emphasise that this assumption is valid assuming that, the boundary layer is fully developed in the water column. In the same study, it is argued that it is not possible to specify the bed-friction coefficient accurately without further modelling of the boundary layer.

Stansby (2006) shows that the wake of a conical island is poorly represented in the two-dimensional (depth-averaged) model when compared to a three-dimensional boundary layer model that is validated against experiments. Their numerical results show vortex shedding wakes are over emphasised in the depth-averaged models, whereas the stable wake length is under estimated. The study concludes that the poor representation of the shallow wakes is due to the amplification of the bed friction coefficient on the solution. Draper (2011) explains that in depth-averaged models the bed friction vector, which leads the bottom current vector, is defined according to the depth-averaged velocity. This implies that the velocity at the seabed is assumed to be always in phase and a constant fraction of the depth-averaged velocity. However, in reality the velocity observed at the bottom will differ by magnitude and possibly in sign (Owen, 1980; Draper, 2011). Thus, the frictional dissipation on the seabed will be delayed in the depth-averaged models.

Use of a three-dimensional model evidently improves the computed velocity profiles, as the model is not bound to use a fixed velocity profile at all times. However, it is important to choose an appropriate turbulence model, so that the vertical and horizontal mixing are computed accurately, which eventually affects the frictional dissipation (Draper, 2011).

Nadaoka and Yagi (1998) emphasise that direct application of such turbulent models in the shallow water models are not realistic mainly due to the large computational areas with different source terms that lead to turbulence (i.e. bottom friction, wind shear stress, etc.), as well as the nature of the turbulent models. The two-equation depth-integrated k-ε turbulence models are most commonly used where free shear layer turbulence and turbulent advection are important (Falconer, 1993). However, the validity of inclusion of turbulence in depth-integrated models is still under investigation.

Model Details

a. Anglesey and Bristol Channel

As explained in WG3 WP6 D4B, a single comprehensive model has been constructed of the southwest coast of the UK including the Irish Sea. The model has three open boundaries, each of which is used for tidal forcing. The first boundary, with the Atlantic to the southwest, is set just beyond the continental shelf. This enables the quarter-wave length resonance effect in the Bristol Channel to be captured. The second boundary is located at the western end of the English Channel. The third is at the North Channel between Ulster and Galloway. Semi-diurnal M_2 and S_2 tidal constituents are used to force the model at the open boundaries. It is assumed that the water levels at these boundaries are unaffected by the disturbance caused by the presence of tidal turbines in the interior of the domain.

As for the Anglesey site, the inter-tidal zones along the Cumbrian and Lancashire coasts are included in order to model the reflected waves directed towards the eastern Irish Sea. Similarly, the inter-tidal zones around the Severn Estuary are also included

in the model. A wetting and drying treatment is used to model the moving shoreline in the inter-tidal zones, following Bunya *et al.* (2009).

The mesh is unstructured except in the regions where rows of tidal turbines are to be deployed. Within these areas a structured mesh of elements is embedded. The mesh size is varied due to the regions of interest. Figure 1 shows the portion of the mesh focusing on the Welsh coasts of the UK including the Anglesey headland and the Isle of Man. Figure 2 shows the mesh around the Bristol Channel region. In the Bristol Channel mesh, Lundy and the Flat Holm and Steep Holm islands are included in the model.

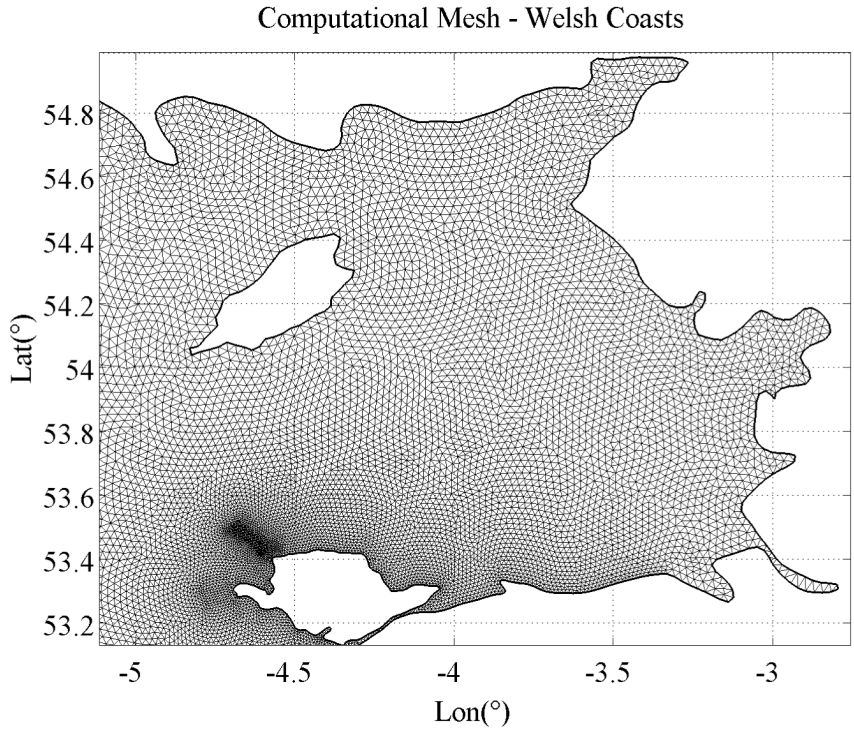

Figure 1 Two-dimensional unstructured triangular mesh focusing on the Irish Sea in the region of the Cumbrian and Lancashire coasts

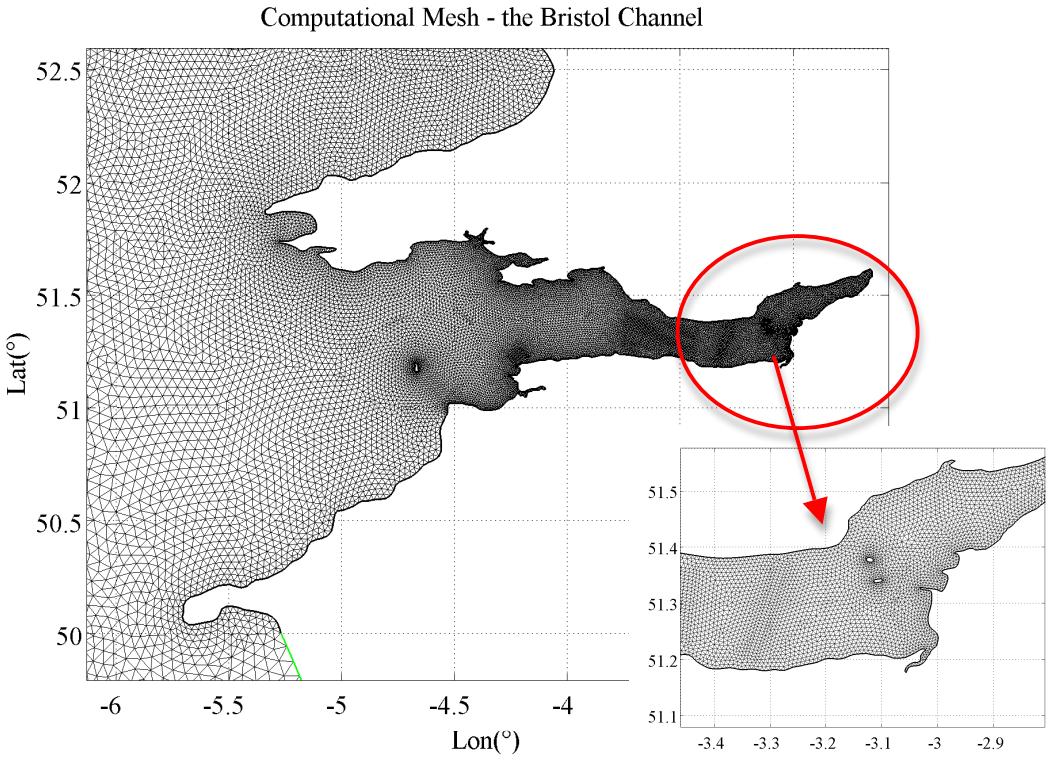

Figure 2 The unstructured triangular mesh of the Bristol Channel. A zoomed in section focusing on Flat Holm and Steep Holm is also shown.

A quadratic bed friction term is applied within the model, with the local bed stress components given by,

$$\tau_x = \rho C_D u\sqrt{u^2+v^2}, \qquad \tau_y = \rho C_D v\sqrt{u^2+v^2}, \tag{1.1}$$

where ρ is the density of seawater, C_D is the drag coefficient and, u and v are the horizontal depth-averaged tidal current velocity components. In calibrating the model, the best fit to field observations after harmonic analysis was obtained by setting C_D = 0.0025. The model was run for a complete spring-neap cycle.

b. Pentland Firth

The model developed to analyse the Pentland Firth is described and validated in WG3 WP6 D4A. The model has many similar features to that of the model used in analysing Angelsey and the Bristol Channel. Like this model an unstructured mesh is

used but in the area of the Pentland Firth structured elements are included to allow turbines to be located. The mesh used is shown in Figure 3 with details shown in Figure 4.

A difference between the model used for Angelsey and Bristol Channel, and that used to study the Pentland Firth is that no wetting and drying is applied in the latter model. The area of the Pentland Firth model includes a small inter-tidal zone, which is found to make no significant difference in accurately simulating the tides occurring in the region. Thus, the model excludes the wetting and drying treatment in the solution.

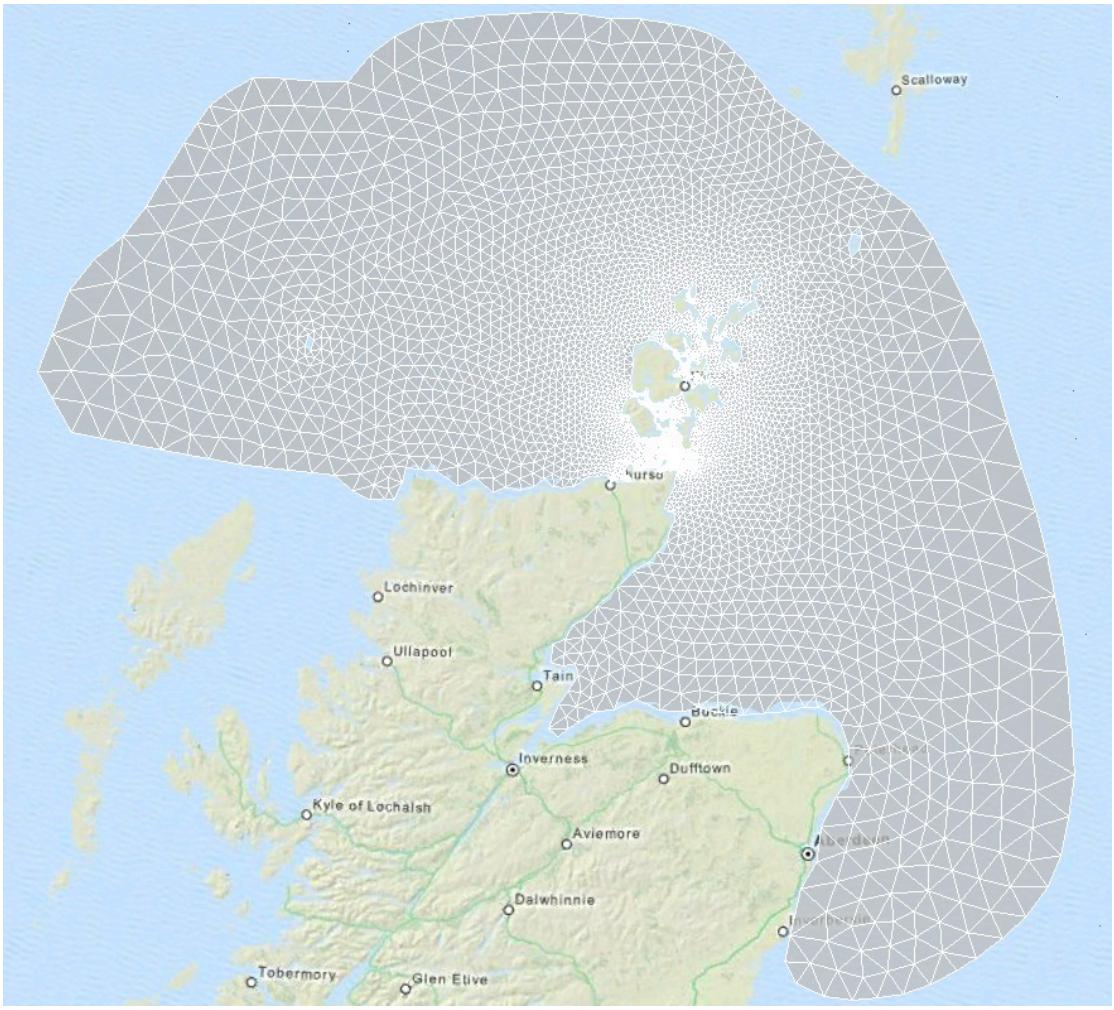

Figure 3 Mesh used in Pentland Firth study

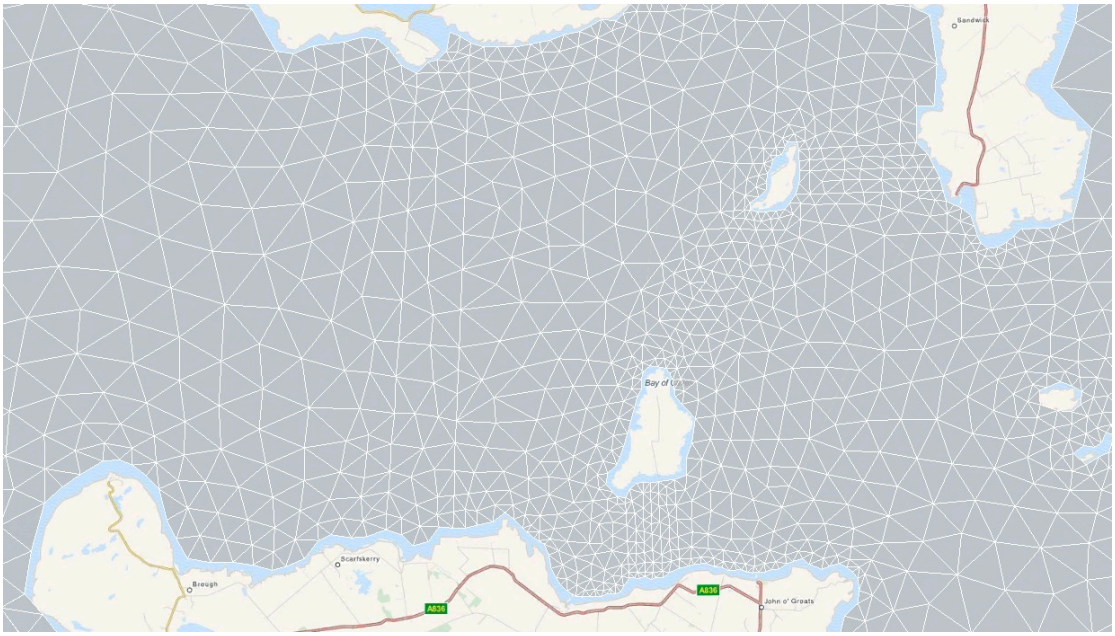

Figure 4 Details of mesh in region of the Pentland Firth

2. Anglesey Skerries

This section considers firstly the validation of the model focusing on the Anglesey Skerries region and secondly analysis of the available power that can be generated using various array configurations. Analysis is also presented on the change of M_2 tides to investigate the effect of tidal array deployments in the vicinity of the areas of interest.

Tidal Hydrodynamics

In a previous study of the tidal dynamics of the model area, Howarth (1984) found the Irish Sea to be a small system that does not respond directly to geophysical forces. Thus the naturally occurring currents in the Irish Sea are mainly driven by the interaction between two tidal waves: one from the Atlantic Ocean entering through St. George's Channel, the other entering through the Malin Shelf Sea and the North Channel.

Model Validation

Validation of the models created for each site has been described in WG3 WP6 D4A and WG3 WP6 D4B. Here, improved results are presented owing to the tuning of the model parameters (bed friction coefficient and eddy viscosity) and inclusion of the

wetting and drying treatment in the model. For brevity, the results considering that are closer to the observations are given in this report.

a. Water Levels

In terms of water surface elevation, model validation was undertaken against observed data obtained from the Admiralty Tide Tables for M_2 (Table 2) and S_2 (Table 3) constituents (Admiralty Charts, 1997). The model results are in very close agreement with the observations for both amplitude and phase. The water level amplitudes agree to within 5% and the small phase differences suggest that the model predicts the time of high water correct to within eight minutes.

Table 2 Tidal harmonic analysis comparisons for M_2 constituent

Location	*Coordinates*	*Observations*		*DG-ADCRIRC*	
		$H_n(m)$	$\varphi_n(^\circ)$	$H_n(m)$	$\varphi_n(^\circ)$
Holyhead	53° 19'N 04° 37'W	1.81	292	1.80	292
Cemaes Bay	53° 25'N 04° 27'W	2.13	307	2.12	304
Amlwch	53° 25'N 04° 20'W	2.30	305	2.26	307
Moelfre	53° 20'N 04° 14'W	2.47	308	2.42	311
Trywn Dinmor	53° 19'N 04° 03'W	2.47	310	2.49	312
Beaumaris	53° 16'N 04° 05'W	2.57	312	2.51	313
Port Trecastell	53° 12'N 04° 30'W	1.50	278	1.57	277
Trearddur Bay	53° 16'N 04° 37'W	1.56	280	1.61	280

The model results indicate that the tidal range differs significantly between the Irish and Welsh-English coasts. This behaviour is also discussed by Howarth (1984), and it was suggested that the main reason for this difference is the Coriolis force, which deflects the propagating wave towards the eastern Irish Sea.

Table 3 Tidal harmonic analysis comparisons for S_2 constituent

Location	*Coordinates*	*Observations*		*DG-ADCRIRC*	
		$H_n(m)$	$\varphi_n(^\circ)$	$H_n(m)$	$\varphi_n(^\circ)$
Holyhead	53° 19'N 04° 37'W	0.59	329	0.59	333
Cemaes Bay	53° 25'N 04° 27'W	0.71	345	0.67	345
Amlwch	53° 25'N 04° 20'W	0.75	345	0.71	350
Moelfre	53° 20'N 04° 14'W	0.81	348	0.76	354
Trywn Dinmor	53° 19'N 04° 03'W	0.80	351	0.78	356
Beaumaris	53° 16'N 04° 05'W	0.82	356	0.79	357
Port Trecastell	53° 12'N 04° 30'W	0.50	320	0.53	317
Trearddur Bay	53° 16'N 04° 37'W	0.54	315	0.54	320

Harmonic analysis of the model predictions indicates that degenerate M_2 and S_2 amphidromes are generated off the east coast of Ireland. Figure 5 shows the predicted M_2 tidal constituent amplitude distribution, locating the amphidromic point (indicated by the dark blue region). It is stated by Pugh (1987) that this amphidromic system transmits tidal energy towards the north of the Irish Sea, where a standing wave forms, enhancing the tidal amplitudes towards the Welsh coasts.

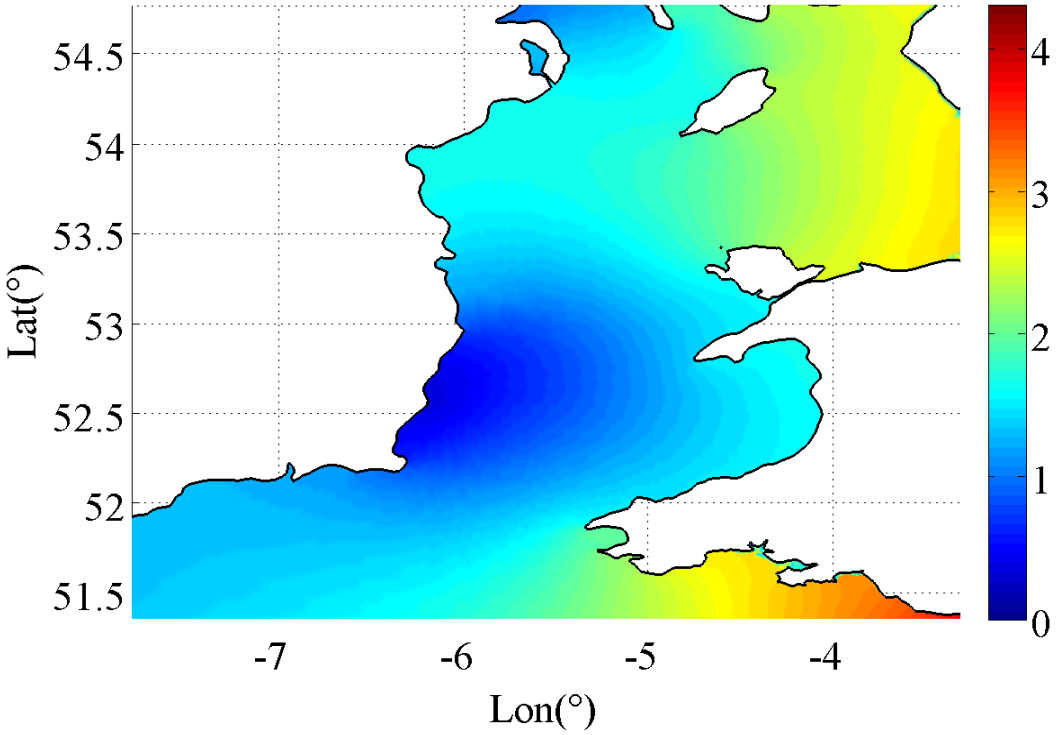

Figure 5 M_2 tidal amplitudes in the Irish Sea obtained from harmonic analysis of the predicted water levels.

b. Currents

Measurements of tidal currents are more susceptible to noise and tend to be of shorter duration than measurements of water levels (Pugh, 1987). The reliability of the recorded current data is also affected by the elevation of the velocity gauge above the seabed (Godin, 1983). Data acquired near the seabed are highly sensitive to the exact nature of the local boundary layer, which in turn means that the extrapolation of such data to depth-averaged values is not robust. Current amplitude comparisons are possible using measurements recorded closer to the top of the water column. In this report, the field current data are related to the depth-integrated current in the model using the $1/7^{th}$ power law profile, as the actual profile is unknown.

The observed data are obtained from the British Oceanographic Data Centre. The coordinates of the selected gauge are 53°17'N 4°55'W, located northwest of Holyhead. The bathymetric depth is 44.0 m, and the readings were conducted 31.0 m above the sea floor.

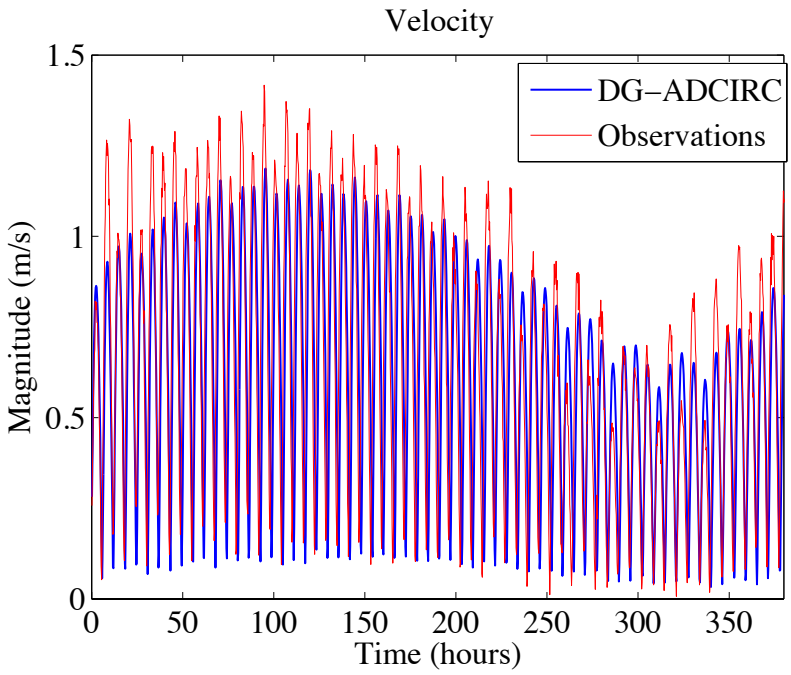

Figure 6 Predicted and observed tidal current magnitude time histories at a gauge north-west of Holyhead.

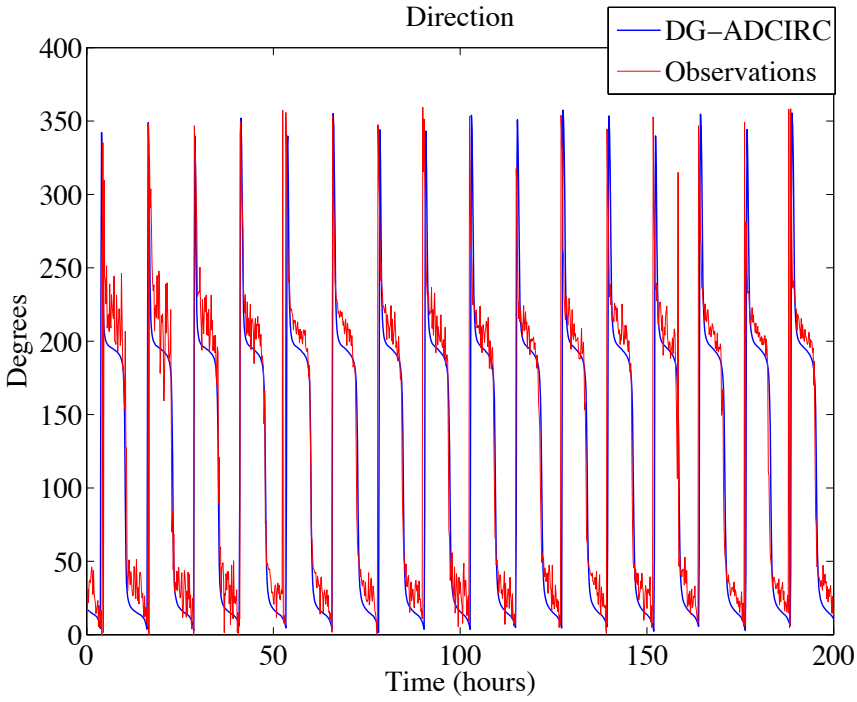

Figure 7 Predicted and observed tidal current direction time histories at a gauge north-west Holyhead.

Figure 6 displays the predicted and observed tidal velocity magnitude time histories; Figure 7 shows the corresponding tidal current directions with time. During ebb tide the flow velocity is under-predicted, whereas during spring tide it is over-predicted. A possible explanation for this discrepancy might be the bed-friction coefficient applied in the model. The level of agreement shown here indicates that the model is capturing the dominant tidal hydrodynamics. There are several possible causes for the discrepancy, including noise in the field measurements. Furthermore, it is well known that depth-averaged models do not capture all the physics of the flows around a headland (Stansby, 2006).

Power Analysis

This section describes the parametric study for assessing the available power in the vicinity of the Anglesey Skerries. In WG3 WP6, the effect of turbine devices on the local flow field is represented by a line sink of momentum, following Draper (2011). The parametric study is undertaken to examine the effects of location and connectivity of the arrays for specified local blockage ratio and wake velocity coefficients, α_4, on the available power.

Using LMADT, for prescribed flow conditions, local blockage ratio (B), and wake velocity coefficient (α_4), it is possible to compute the time series of power available to the turbines and the total power removed from the stream. As explained by Vennell (2011), there is an optimum wake velocity coefficient that maximizes the available power. This value is dependent on the turbine arrangement as well as the coastal features near the area of interest, and the optimum value may vary through the spring-neap cycle (Adcock *et al.*, 2013). However, here we employ a constant wake velocity coefficient throughout the cycle, so that the calculated values will be slightly less than the maximum that would be determined if a variable wake velocity coefficient were to be taken into account. In the present analysis, a range of wake velocity coefficients is considered in order to evaluate the optimum α_4 value from which to compute the maximum available power.

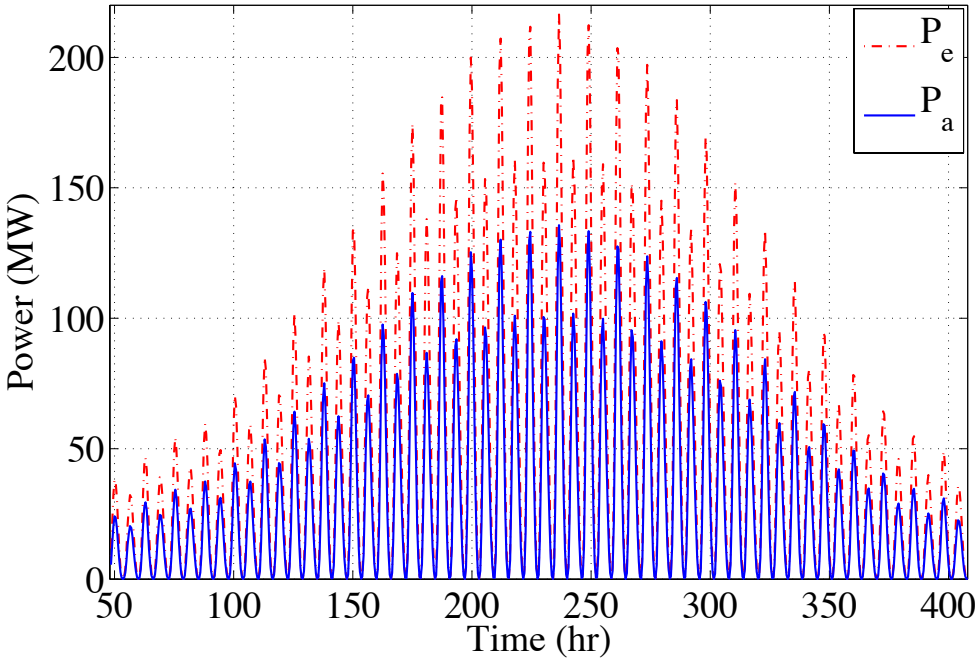

Figure 8 Raw data time series indicating the power extracted from the stream and power available to the turbines for B=0.5 α_4=0.5, and array configuration ASA1+ASA2.

Figure 8 presents the raw power data obtained from a particular test case for a spring-neap cycle. The figure shows the raw data that accounts for the power available to the turbine arrays (P_a) and the total power that is extracted from the stream (P_e). In this case, $B = 0.5$ and $\alpha_4 = 0.5$ for the specific array configuration, ASA1+ASA2 (see Figure 10 for array locations).

Averaging the obtained available power over a tidal cycle and repeating the same procedure for each α_4 for a fixed B, it is possible to evaluate the optimum wake velocity coefficient. This is achieved by fitting a spline to the averaged power values (Figure 9). In the rest of this report, the results are presented for the optimum wake velocity coefficients, α_4 – *i.e.* when the available power is maximized.

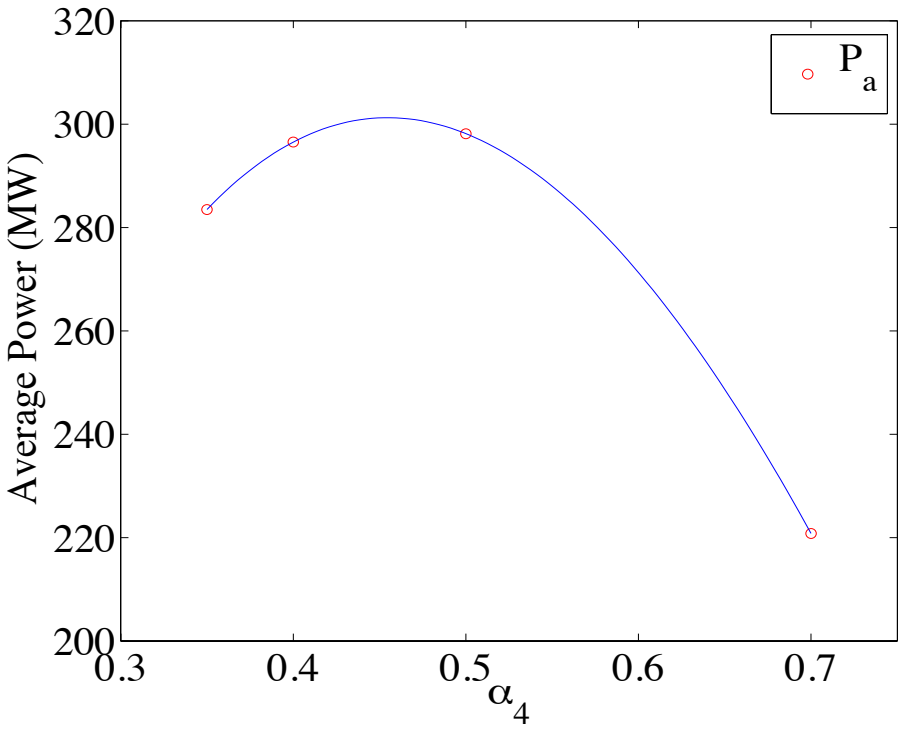

Figure 9 Evaluation of the maximum power (P_a) with respect to averaged power values obtained for different α_4 for B=0.5 and array configuration ASA1+ASA2

a. Location

The naturally occurring flow around a headland with realistic bathymetry is highly complex, and so the optimum location to install an array of tidal devices is not obvious. Whilst it may appear reasonable at first sight to use the undisturbed kinetic energy flux to guide the location of turbine array deployments (Draper *et al.*, 2011), this can be further complicated by the existence of turbines causing flow diversion (see Hydrodynamic Effects). Figure 10 indicates several trial locations for tidal turbine deployment offshore of the Skerries. The area selected for the analysis is based on two factors. First, the naturally occurring kinetic energy flux is relatively higher than other regions around the Anglesey headland. Second, the bathymetry of the area is favourable for tidal farm deployment.

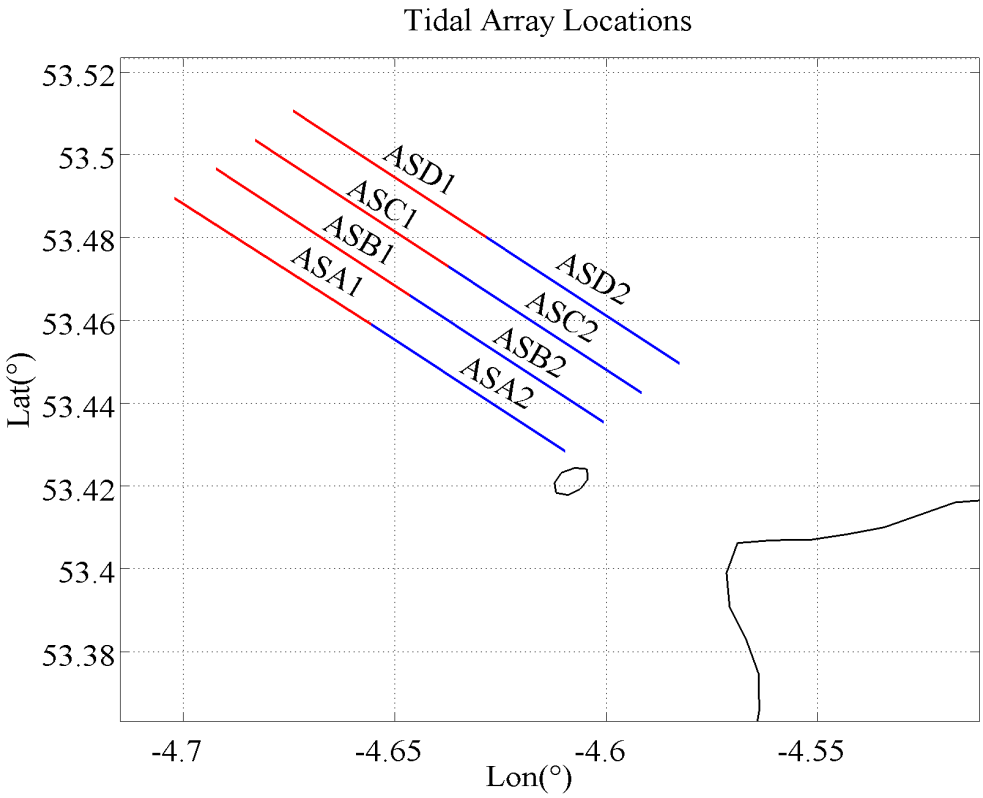

Figure 10 Selected locations of tidal turbine arrays extending towards NE of the Anglesey Skerries

The nomenclature for array configurations is based on the placement of the arrays in the SW-NE direction (ASA being the furthest SW and ASD the furthest NE) and how far the arrays are located away from the Anglesey coastline. Arrays that are further offshore are labelled as Region 1, and those closer to the Skerries as Region 2. Each array has a total length of 4.5 km and is placed approximately 1 km apart from the next array. The arrays are located in regions with varying depths. From Table 4 it can be seen that the mean depths in Region 1 are greater than in Region 2. Hence, the arrays in Region 1 have a larger swept area of turbines compared to the turbines located in Region 2, when working with a specified local blockage ratio.

Table 4 Power values for different blockage ratios at optimum wake velocity coefficients

Location	Blockage	Opt. α_4	$P_{available}$ (MW)	$P_{extracted}$ (MW)	Average Depth (m)
ASA1	0.1	0.35	12.7	20.5	55.4
	0.3	0.37	54.7	97.7	
	0.5	0.46	124.3	211.3	
ASB1	0.1	0.35	11.3	18.1	57.5
	0.3	0.37	48.6	87.4	
	0.5	0.45	112	192.9	
ASC1	0.1	0.35	10.9	17.5	54.9
	0.3	0.37	46.5	83.1	
	0.5	0.46	106.3	181.5	
ASD1	0.1	0.35	10.6	17.1	53.3
	0.3	0.37	45	80.4	
	0.5	0.46	101.9	172.1	
ASA2	0.1	0.35	17.2	27.7	36.3
	0.3	0.39	70	122	
	0.5	0.50	145.3	230.1	
ASB2	0.1	0.35	16.6	26.8	37.8
	0.3	0.39	67.3	116.6	
	0.5	0.49	139.8	222.8	
ASC2	0.1	0.35	13.5	21.8	43.6
	0.3	0.39	57.1	99.9	
	0.5	0.48	124.5	202.5	
ASD2	0.1	0.35	12.1	19.6	47.2
	0.3	0.38	51.7	91	
	0.5	0.46	116	195.9	

Table 4 summarises the maximum available power and the total power extracted from the sites and for different blockage ratios, obtained for the optimum wake velocity coefficients. In the table, it is evident that arrays placed closer to the Skerries (Figure 12) extract more power when compared to arrays deployed further offshore (Figure 11).

Despite the fact that the turbines in Region 2 have smaller swept areas, they produce considerably more power than the turbines in Region 1. This difference can be shown by calculating the power produced per swept area, which is a metric introduced by Adcock *et al.* (2013). An example for this can be given by focusing on ASA1 and ASA2 turbine arrays. For a high blockage test case (B = 0.5), the power per swept area for ASA1 array is 0.997 kW/m^2, whereas this value is 1.781 kW/m^2 in ASA2. A

similar relationship is observed for other arrays located in different regions when using fixed blockage ratios.

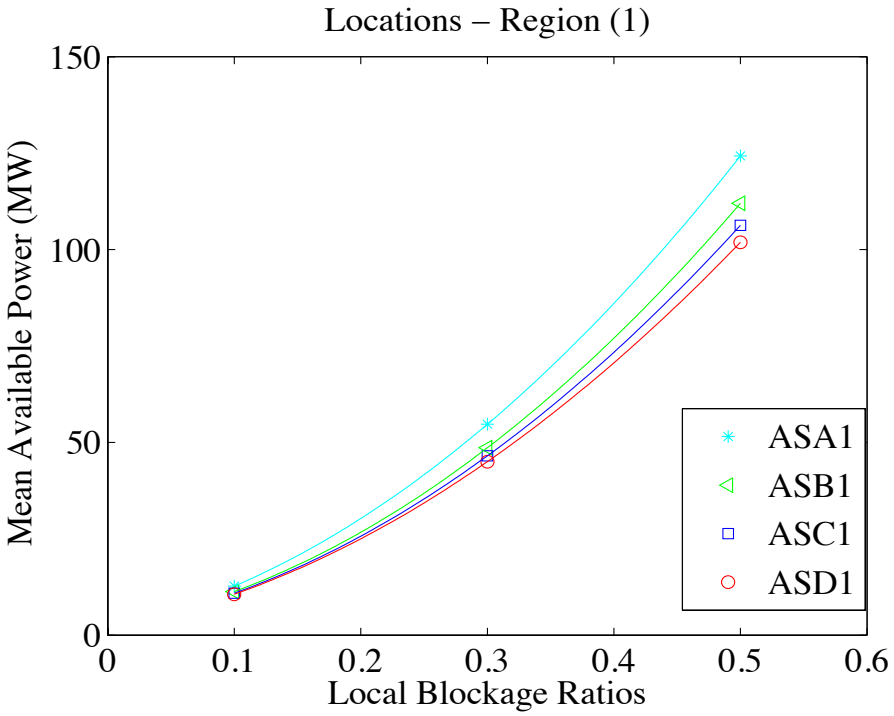

Figure 11 Maximum available power as a function of blockage ratio for the arrays located in Region 1

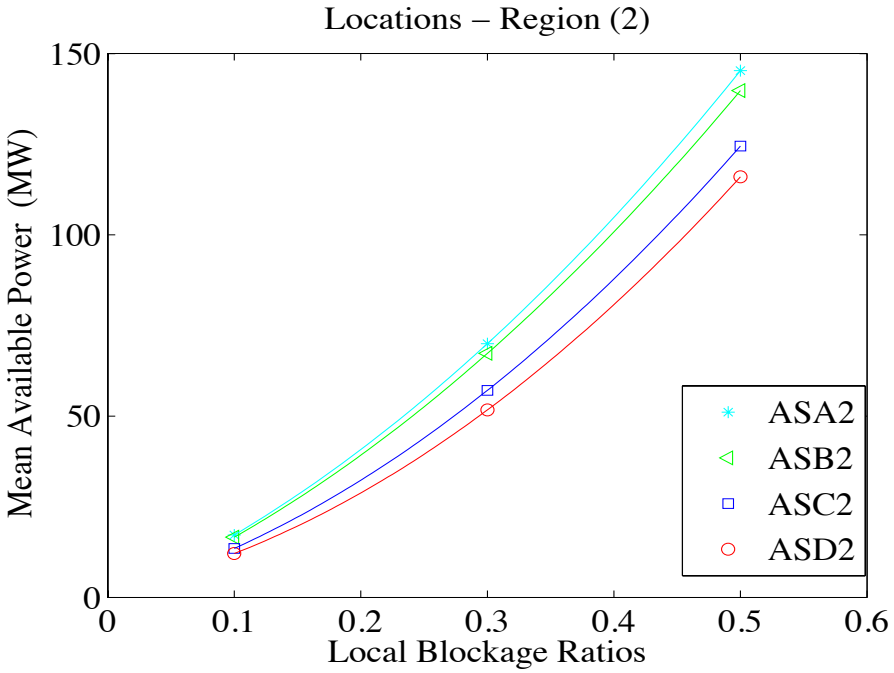

Figure 12 Maximum available power as a function of blockage ratio for the arrays located in Region 2

b. Array Connectivity

This section examines the effect of multiple array deployment on array performance. Studies such as that of Adcock *et al.* (2012) have shown that there is significant interaction between multiple rows of arrays installed at a given site. Here, we investigate the effect of this interaction on the available power. Following the same methodology for computing the maximum available and extracted power values, Table 5 lists the results obtained from several combinations of array deployments. The table considers the maximum available and extracted power values for parallel (*i.e.* ASA1+ASA2) and series array connections (*i.e.* ASA2+ASB2) respectively. Economic gain presented in Table 5 corresponds to the ratio of energy gain by connecting turbine arrays in parallel or in series.

Table 5 Maximum available power estimates for series and parallel array configurations for various blockage ratios

Arrays	*Blockage*	*Opt.* α_4	$P_{available}$ (MW)	$P_{extracted}$ (MW)	*Economic Gain*
ASA1+ASA2	0.1	0.35	30.2	48.7	1.010
	0.3	0.38	130.8	232.5	1.049
	0.5	0.46	301.2	517	1.117
ASB1+ASB2	0.1	0.35	28.1	45.1	1.007
	0.3	0.37	121.8	219.7	1.051
	0.5	0.45	284.5	494.8	1.130
ASC1+ASC2	0.1	0.35	24.6	39.7	1.008
	0.3	0.37	108.4	196.7	1.046
	0.5	0.44	260.3	461.3	1.128
ASD1+ASD2	0.1	0.35	22.9	37	1.009
	0.3	0.36	101.4	185.2	1.049
	0.5	0.44	245.2	434.3	1.125
ASA2+ASB2	0.1	0.35	32.4	52.3	0.959
	0.3	0.44	114.6	183.1	0.835
	0.5	0.58	199.1	280.2	0.698
ASA2+ASC2	0.1	0.35	29.8	48.1	0.971
	0.3	0.42	110.4	181.7	0.869
	0.5	0.56	199.9	289	0.741
ASA2+ASD2	0.1	0.35	28.7	46.2	0.980
	0.3	0.41	109.6	182.4	0.901
	0.5	0.54	205.6	305.7	0.787
ASA2+ASB2+ ASC2+ASD2	0.1	0.36	54.2	86.2	0.912
	0.3	0.48	167.9	253.1	0.682
	0.5	0.64	257	337.6	0.489

Interpreting the results with respect to the array combinations, it is evident that connecting the arrays in parallel is more advantageous. The power available to the turbine in parallel connection is higher than the sum of the two arrays installed in isolation. An example can be given by focusing on the ASA arrays using a high blockage case (B=0.5). When the individual available power values are summed, the total power is found to be 269.6 MW, whereas Table 5 shows that this is an underestimate of the actual value. For the ASA1+ASA2 configuration, the available power is 301.2 MW. There is approximately 12% power gain above the sum of the two individual array configurations. This percentage gain diminishes with decreasing blockage ratio because less thrust is applied to the flow.

For arrays connected in series, the available power reduces. Consider the ASA2 and ASB2 arrays in series for B = 0.5. In this case, the sum of individual available power outputs is 285 MW whereas the maximum available power is computed to be 199 MW. For a highly blocked flow where a large thrust is applied, it is more advantageous to put the arrays in parallel than in series. However, for a low blockage case, as the disturbance to the flow field is reduced; the penalty from placing turbines in series is less severe.

In general, arrays interact constructively when connected in parallel and, interact in a destructive manner when deployed in series.

Hydrodynamic Effects

A primary objective of this research is to evaluate the change in the flow field in the presence of tidal devices. One-dimensional analysis of this problem, using LMADT indicates a head drop due to the power extraction, which leads to an increase in the flow velocity just downstream of the turbines. In the far field, after the wake is recovered, the flow velocity decreases due to the power extraction from the current.

In a two-dimensional numerical model, the wake mixing length is assumed to be much smaller than the element size. Representation of the far-field characteristics of the flow passing through an array of turbines is then possible by inserting a line sink

of momentum within the numerical solution (see WG3 WP6 D5 for implementation). To investigate the change in velocity flow field, let us consider arrays ASA2, ASB2, ASC2 and ASD2 connected in series for B = 0.5.

Figure 13 provides a snapshot of the naturally occurring flood tide in the vicinity of the Anglesey Skerries. The average flow velocity observed in the vicinity of the area is 2.1 m/s. Once the arrays are installed, the flow bypasses the arrays, mainly on the offshore side.

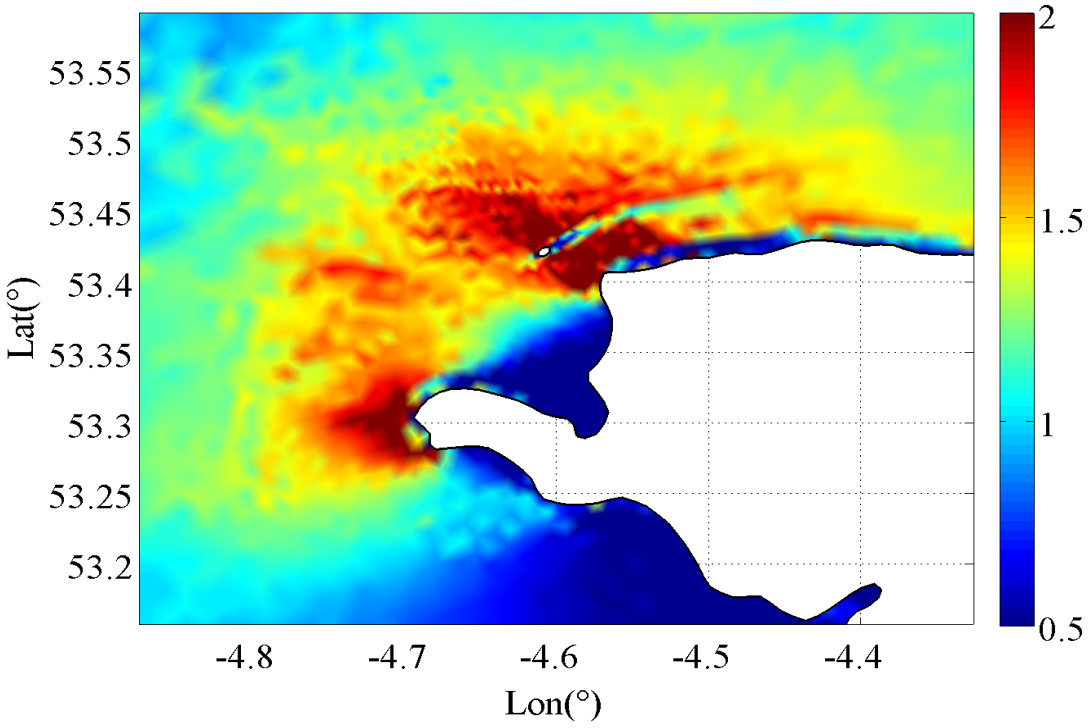

Figure 13 Natural velocity flow field occurring around the Anglesey Skerries (m/s)

Figure 14 shows a snapshot of the flow field in the presence of tidal arrays deployed. It is evident that the arrays provide additional resistance to the flow. Downstream of the arrays, the velocity magnitude decreases significantly due to the power extraction. Figure 15 plots the difference between the two flow fields. It can be seen that the flow diversion is not symmetric and the bypass flow towards the ocean side is more enhanced than in the Skerries region. The flow diversion indicates that the available power is restricted with respect to the thrust applied to the flow in a partially blocked flow regime. The flow disturbance is quantified by computing the change in the M_2

tidal harmonic. We consider an array configuration that gives the maximum total power loss: ASA1+ASA2 parallel array for $B = 0.5$ and $\alpha_4 = 0.5$. The model is run for an entire spring-neap cycle and comparisons are undertaken against natural flow conditions.

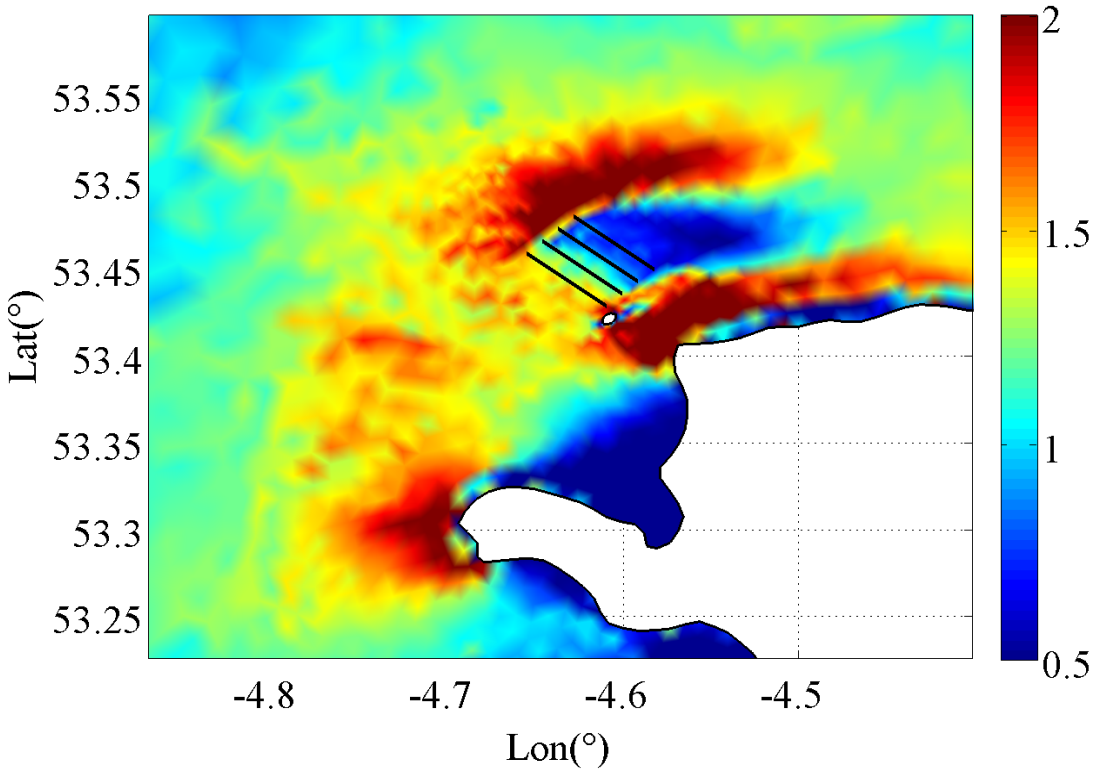

Figure 14 Current velocity plot for a parallel tidal array (ASA2+ASB2+ASC2+ASD2) deployment around the Anglesey Skerries

Harmonic analysis of the model results for the ASA1+ASA2 configuration shows that the change in M_2 amplitudes is less than 3%. Arrays placed to the north of the Anglesey headland have a large influence on the tidal amplitudes around Anglesey Island. Table 6 shows the computed values for the M_2 tidal harmonic constituent at several locations around Anglesey and the Irish Sea. It should be noted that the change is insignificant as far as tidal amplitude is concerned. Figure 16 plots the relevant M_2 amplitude change, focusing on the Anglesey Skerries region.

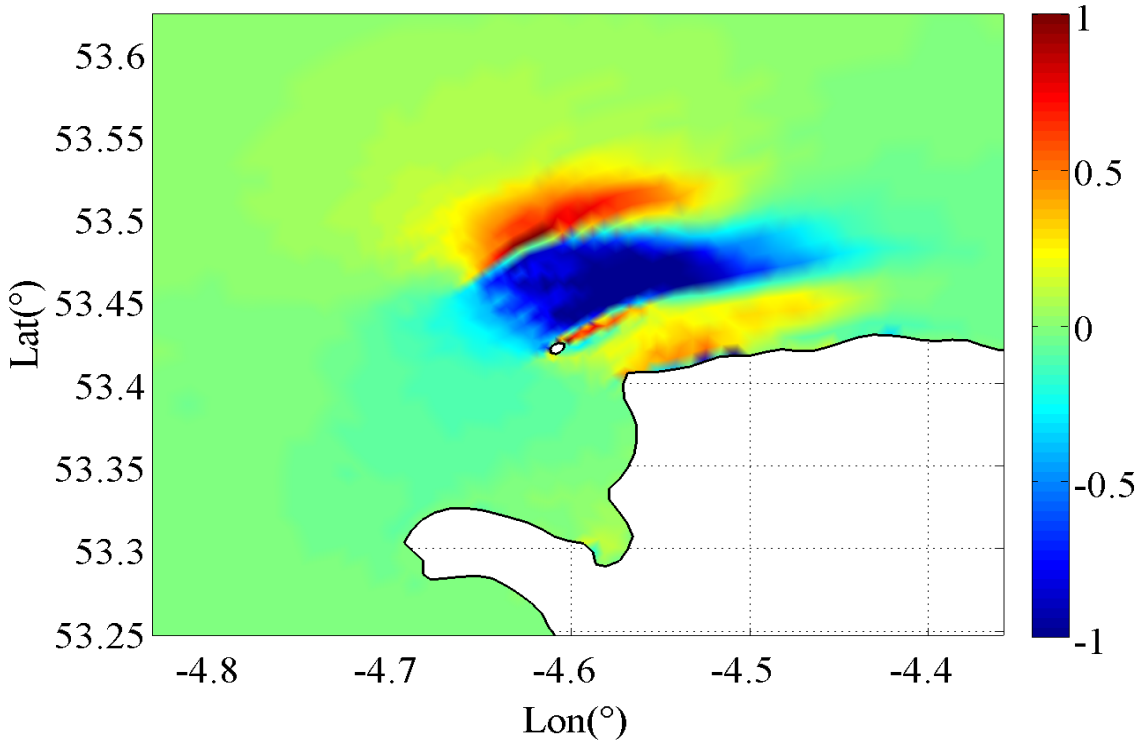

Figure 15 Change in the velocity flow field with respect to the deployment of tidal arrays ASA2+ASB2+ASC2+ASD2

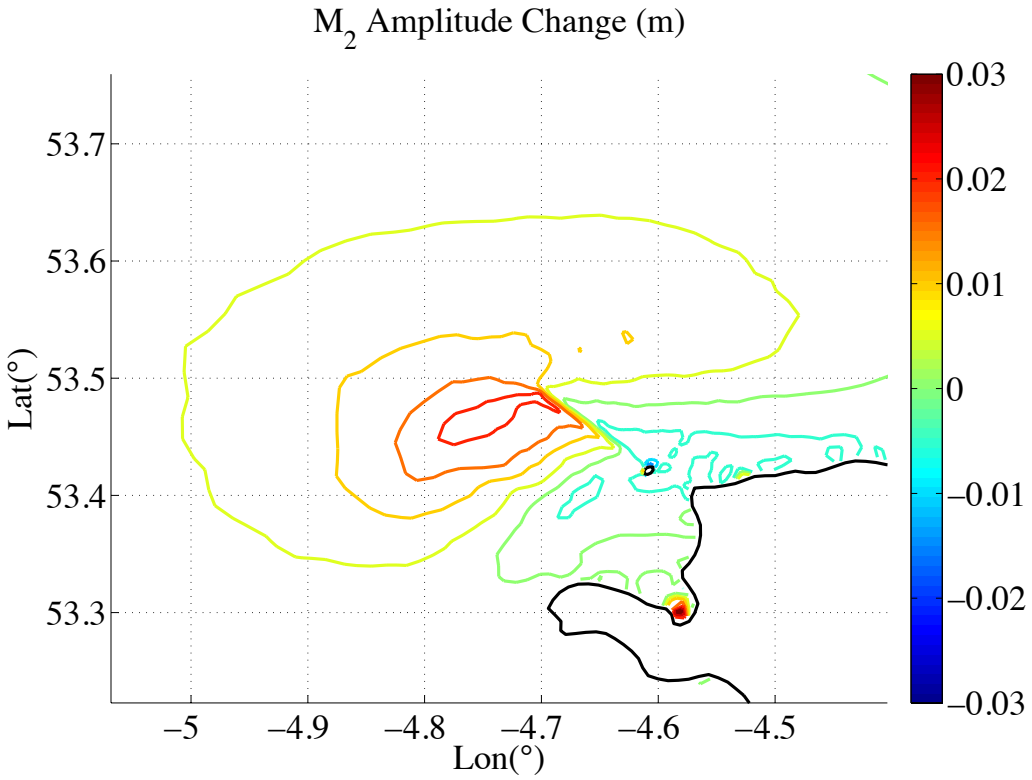

Figure 16 M_2 tidal constituent amplitude change in the vicinity of the Skerries

Figure 17 plots the phase of the M_2 constituent in the Irish Sea, and the change in the vicinity of the arrays is less than 4 degrees. Upstream of the arrays the phase decreases by 2 degrees, whereas an increment of 2.5 degrees occurs downstream. This implies that high tides are delayed by approximately 5 minutes immediately before the array location.

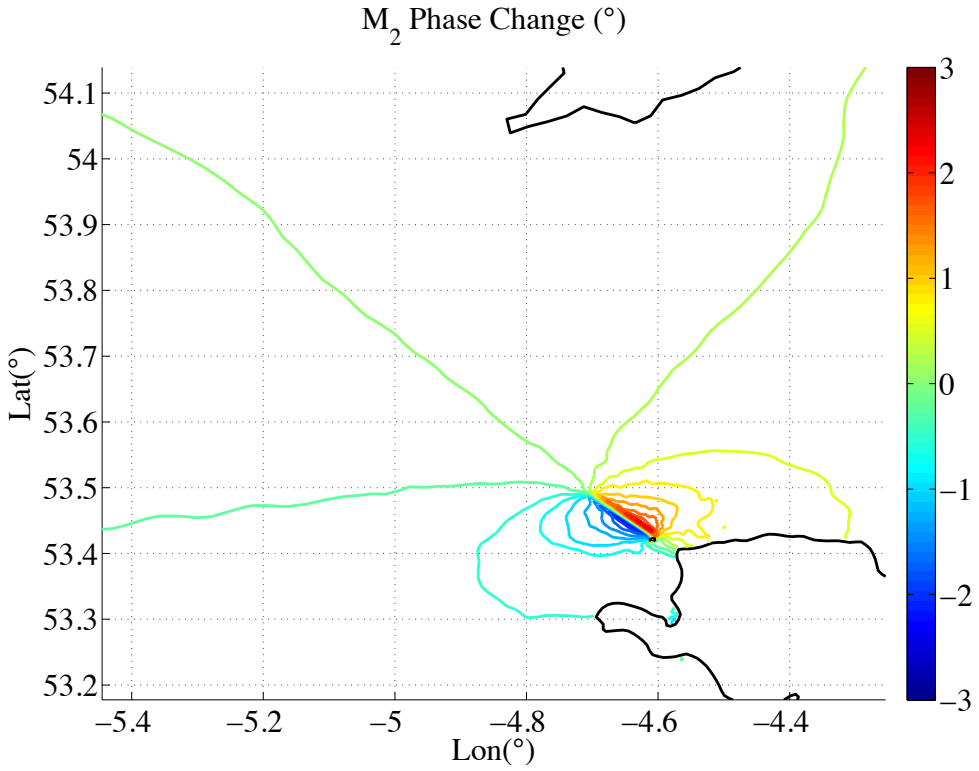

Figure 17 M_2 tidal constituent phase change in the vicinity of the Anglesey headland

Table 6 summarises the model predictions with respect to the M_2 tidal constituent amplitudes and phases. Even for high blockage, the tidal dynamics within the system does not alter significantly.

Table 6 Harmonic analysis of the M_2 constituent for stations around Anglesey and Irish Sea

Location	Coordinates	Natural Case (model predictions)		ASA1+ASA2 for B=0.5	
		$H_n(m)$	$\varphi_n(^\circ)$	$H_n(m)$	$\varphi_n(^\circ)$
Holyhead	53° 19'N 04° 37'W	1.80	292	1.80	291.4
Amlwch	53° 25'N 04° 20'W	2.26	307	2.25	307.5
Trywn Dinmor	53° 19'N 04° 03'W	2.49	312	2.48	312.4
Port Trecastell	53° 12'N 04° 30'W	1.57	277	1.57	276.6
Port St. Mary	54° 02'N 04° 46'W	1.81	323	1.81	323.1
Aberdaron	52° 47'N 04° 43'W	1.41	252	1.42	251.7

3. Bristol Channel

We now consider assessment of the Bristol Channel region for tidal energy development, using similar analysis to that presented in Section 2.

In the literature, several tidal barrage schemes have been considered in order to exploit the rise and fall of the tides in the Bristol Channel. Recent work conducted by the U.K. Government (2010) shows that a tidal barrage scheme could provide 5% of the total electricity demand in the U.K. However, such a barrage would incur very high capital costs compared to other kinds of renewable energy technologies. Another concern for constructing a barrage in the Channel arises from the environmental impact is considered. Overall, the U.K. Government report concludes that it is unfeasible to invest any tidal barrages in the Channel to accomplish the UK renewable energy production goals by 2020.

Tidal turbine arrays offer an alternative to a tidal barrage in the Bristol Channel. The present work aims to evaluate the maximum available power that can be generated by tidal arrays in the Bristol Channel. The present assessment also considers the change

in the local hydrodynamics by focusing on the M_2 tidal constituent, which is representative of the average tidal regime in the Channel.

Tidal Hydrodynamics

A previous study focusing on the tides occurring in the Bristol Channel emphasises that the circulation in the Channel, as well as the Irish Sea, is mainly due to tidal movements (Uncles, 1983). The same study indicates that semi-diurnal tides are predominant in the region, in which M_2 tides are representative of an average tidal cycle. The secondary tidal constituent is S_2, which is approximately 35% of the M_2 tidal constituent regarding both the elevations and currents.

The observed tidal range in the Channel is almost 10 m and the current speed can exceed 2 m/s. Previous studies have shown that two primary factors contribute to the high tidal range observed towards the head of the Channel. Using a simple model, Taylor (1921) found that the sudden change in the channel width and depth cause a funnelling effect, which amplifies the tidal elevations. The other factor is the quarter wavelength resonance effect between the boundary to the Atlantic and the head of the Channel (Fong and Heaps, 1978). In their study, Fong and Heaps (1978) found that the possible resonance is not only dependent on the length of the Channel but also on the resonant period, which is in the semi-diurnal tidal band.

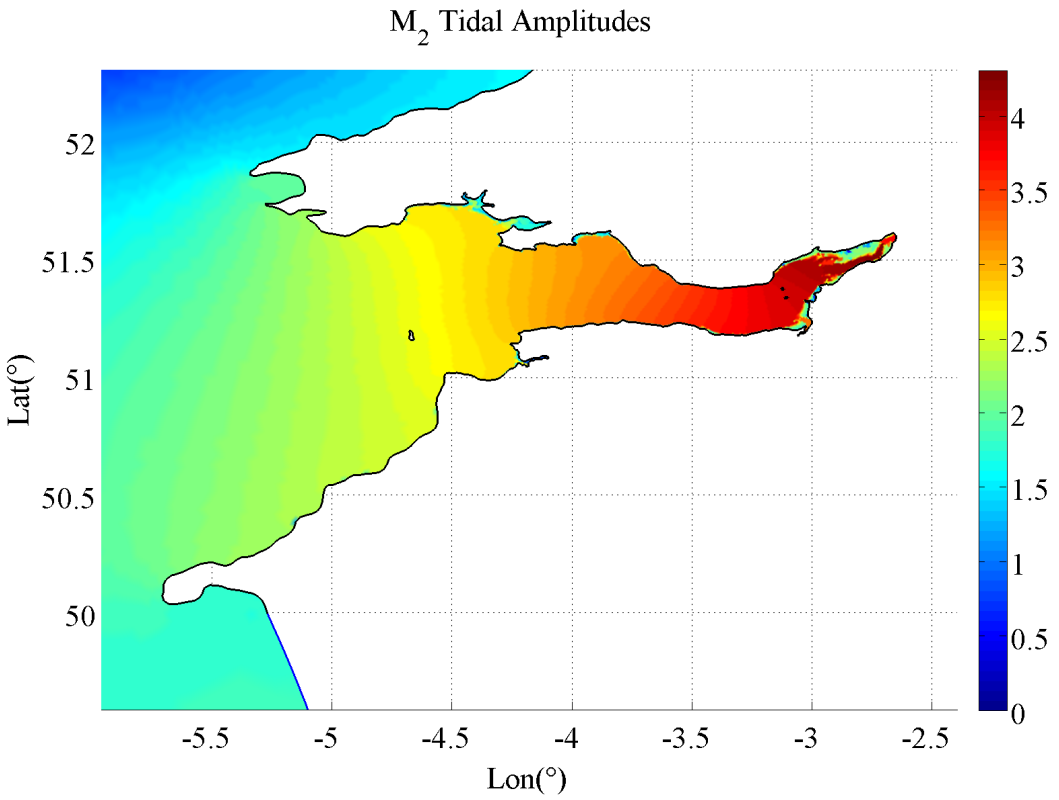

Figure 18 Computed M_2 tidal amplitudes around the Bristol Channel region (magnitudes are in meters)

Figure 18 and Figure 19 show the simulated co-amplitude map and co-tidal lines in the Bristol Channel. The model includes a wetting and drying treatment in order to account for the moving boundary problem. For this reason, conducting a tidal harmonic analysis on the regions, which dries out during ebb tide, shows an abrupt change in the elevations and phases. A brief comparison is given in Table 7, which shows the amplitudes and phases of M_2 tides observed and simulated at several stations across the Channel.

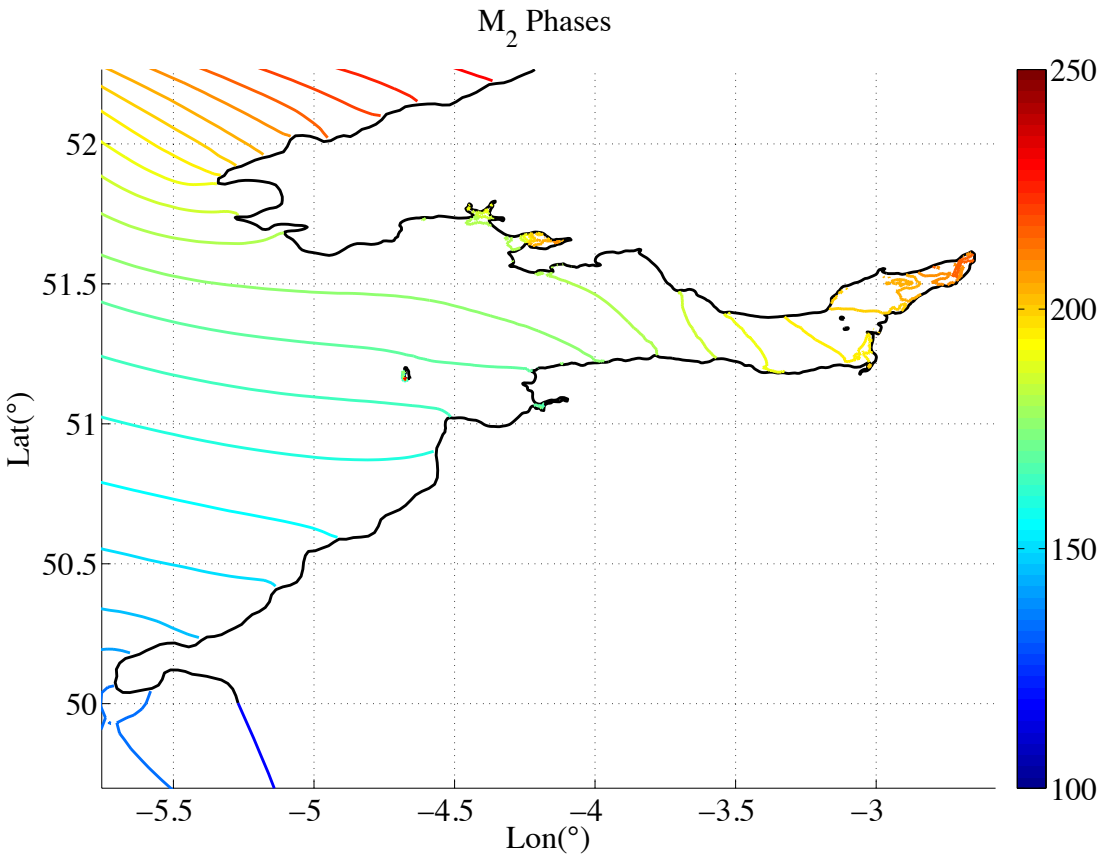

Figure 19 Computed M_2 co-tidal lines in the Bristol Channel

The model over-estimates the phases. The maximum difference between the observed and modelled phases is 10°, which indicates approximately a 20 minute delay in predicting the time of the high water. A similar discrepancy has been discussed by Owen (1980). The study concludes that the observed difference is due to the limitations of using a depth-averaged shallow water model.

The bottom current, which leads the frictional dissipation, cannot accurately be modelled in a depth-averaged model, resulting in over-prediction of the phase (Owen, 1980). The predicted M_2 amplitudes are, however, usually less than the observed values. The error is within a reasonable limit (~ 5%), and thus is not of concern with respect to model accuracy. When moving from east to west of the Channel, the M_2 amplitudes increase rapidly from 2.20 m to 4.20 m. In the entrance of the Bristol Channel the M_2 phase is around 150°, and it increases to 200° towards the head of the

Channel. This change indicates that high water occurs within less than 2 hours throughout the Channel.

Table 7 Comparison of the computed and observed M_2 tidal amplitudes and phases around the Bristol Channel

Location	*Coordinates*	*Observations*		*DG-ADCRIRC*	
		$H_n(m)$	$\varphi_n(^\circ)$	$H_n(m)$	$\varphi_n(^\circ)$
St. Thomas Head	51° 24'N 02° 56'W	4.25	194	4.04	197
Flat Holm	51° 23'N 03° 07'W	Varies	190	3.92	199
Steep Holm	51° 20'N 03° 06'W	3.87	186	3.90	197
Barry	51° 23'N 03° 16'W	3.82	185	3.77	196
Hinkley Point	51° 13'N 03° 08'W	3.80	185	3.85	194
Minehead	51° 13'N 03° 28'W	3.59	183	3.61	188
Ilfracombe	51° 13'N 04° 07'W	3.04	162	2.97	172
Swansea	51° 37'N 03° 55'W	3.19	173	3.13	182
Milford Haven	51° 42'N 05° 03'W	2.22	173	2.24	180
Lundy	51° 10'N 04° 39'W	2.67	160	2.59	169

Figure 20 shows the M_2 current semi-major axes orientation in the Bristol Channel. The figure indicates that the M_2 semi-major axes increased towards the Channel around Minehead as the breath decreases (funnelling effect). Towards to the top of the Channel (bay region) the current magnitudes decrease. Uncles (1981) notes that the observed decrease is mainly due to larger frictional drag applied in the shallower water.

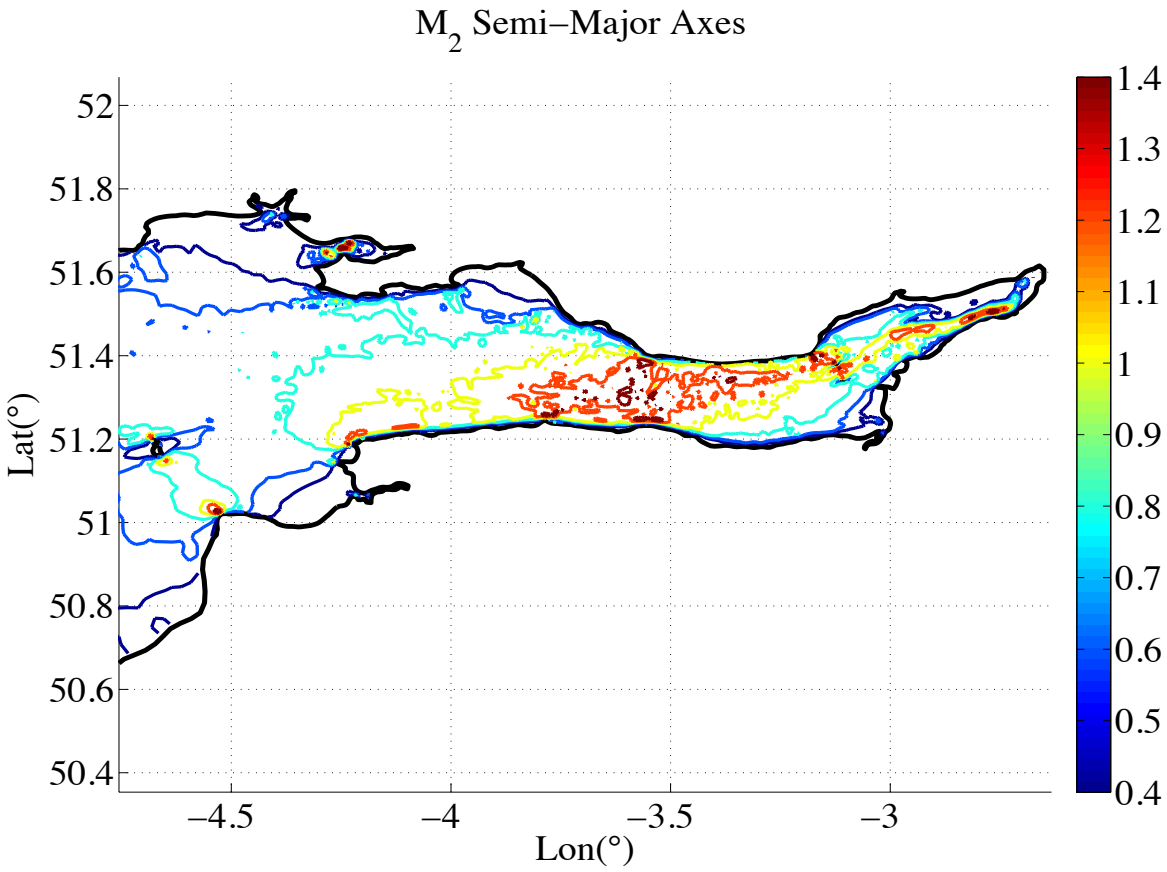

Figure 20 Computed M_2 semi-major axes (magnitude in m/s)

Owen (1980) presents a comparison for east-going and north-going components of M_2 tides observed at two locations. The first of these locations is towards the north of Lundy Island (Station NL: 51° 19'N; 4° 44'W) and the second one is near the Swansea Bay (Station SB: 51° 27'N; 3° 52.5'W). Table 8 shows the observed data taken from the mentioned study and the results obtained from the present depth-averaged model. The east-going components for both stations are in good agreement with the observations. The north-going components, however, are 30 to 40 per cent overestimated in the model. The observed discrepancy is likely to be related to the current recordings. As explained in the Anglesey section, the observations are taken by recording the direction and magnitude of the currents. Thus, even a small error in direction would cause a large error in the magnitude of the velocity components. Bearing in mind that the east-west component is approximately five times larger than the north-south direction, it is evident that the model estimates the dominant direction accurately.

The computed phases are within 4% error (~ 8 min delay) for NL station, and 8% error (~ 16 min delay) for SB station. The predicted phases are within an acceptable error limit.

Table 8 Comparison of observed and calculated M_2 tidal currents in east and north directions

Station	*-z/h*	*Direction*	*Observations*		*DG-ADCIRC*	
			$H(m/s)$	$\varphi(^\circ)$	$H(m/s)$	$\varphi(^\circ)$
NL	0.52	East	0.64	87	0.62	91
		North	0.13	126	0.22	130
SB	0.56	East	0.80	93	0.84	102
		North	0.13	283	0.19	289

Power Analysis

This subsection summarises the parametric study conducted to estimate the maximum available power from the Bristol Channel region. As described in Section 2, the analysis herein also considers the influences of array location and array connectivity on available power. The arrays are described in the LMADT model using the blockage ratio (B), the wake velocity coefficient (α_4) and the upstream Froude number (Fr). The maximum available power and maximum extracted power values are calculated for the optimum wake induction factor. The optimum α_4 has been calculated by fitting a spline to the available power values averaged over a tidal cycle, obtained for different wake induction factor values using a constant blockage ratio (Adcock *et al.*, 2013).

a. Location

High tidal ranges occurring in the Bristol Channel are mainly due to the funnelling effect as well as the resonance between the Atlantic Ocean boundary and the head of the Channel. The analysis conducted for the Anglesey Skerries has shown that there is a slight change in the local hydrodynamics in the region where tidal turbine arrays have been placed. Consideration of any array deployment in the Bristol Channel will also necessitate quantification of the change to the naturally occurring tides, which is influenced by the resonance effect.

Adopting the naturally occurring kinetic energy flux methodology in the Bristol Channel, there are two regions, which indicate favourable places for tidal array deployment. The first of these is the area between Lundy Island and Hartland headland. Given that a detailed investigation of a headland as a tidal energy resource has already been undertaken for the Anglesey Skerries, the above-mentioned region is considered to be a secondary tidal resource development site and so will not be considered for further investigation in this report.

The second favourable area is between Minehead and Barry, which is the narrowest part of the Channel. The computed velocities reach 2 m/s and the average depth is approximately 30 m. The locations for the tidal arrays considered are given in Figure 21. The array placed at the narrowest section of the Channel is BCL0, which is taken as the base test. The rest of the arrays are deployed sequentially from the far west of the Channel where fast flows occur towards to the east. Each array is approximately 14 km long and they are 5 km apart from each other except BCL3, BCL0 and BCL4 arrays. BCL0 array is located in between BCL3 and BCL4 arrays.

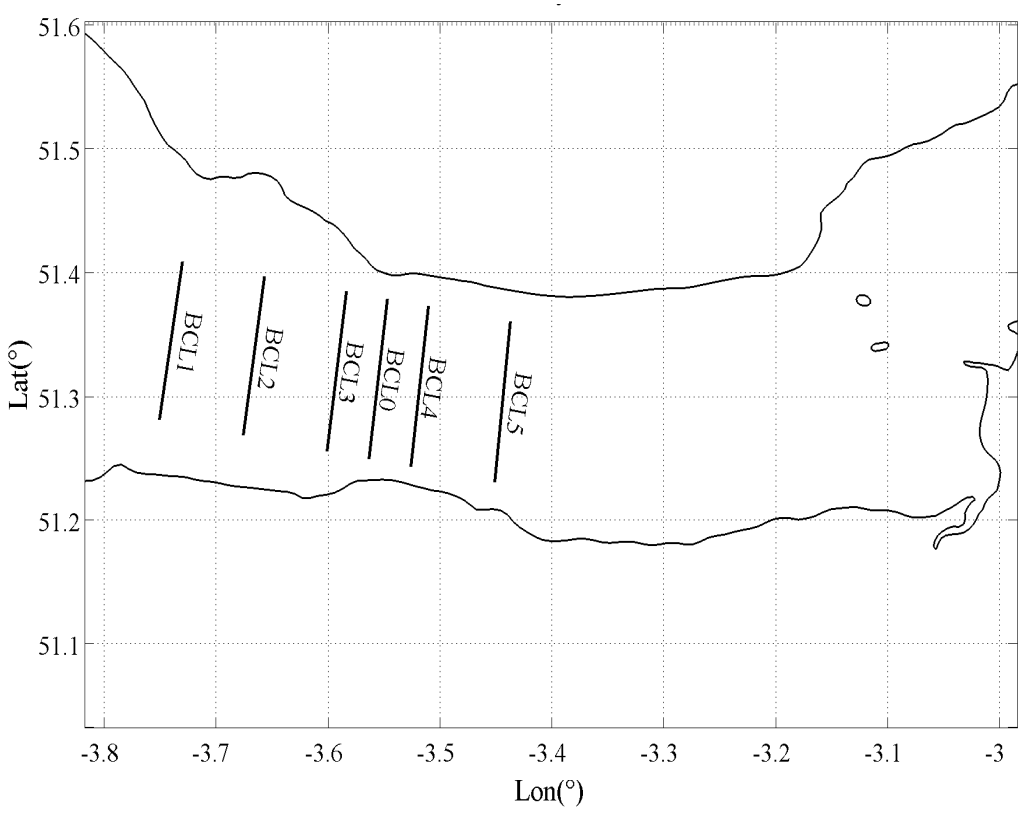

Figure 21 Array locations considered in the Bristol Channel

A parametric study has been conducted for the aforementioned tidal arrays for various wake velocity coefficients (α_4) with fixed blockage ratios. In this work four different α_4 values have been considered, which are 0.35, 0.40, 0.50 and 0.70. Table 9 summarises the maximum available power that can be generated for different blockage ratios at the computed optimum wake velocity coefficients. Considering the maximum available power values, it is seen that BCL3 performs better for all cases. The optimum α_4 values are increased slightly as the blockage is increased, but they do not exceed 0.40. For BCL0 array, the array efficiencies ($\eta_{turbine} = P_{available} / P_{extracted}$) are closer to that of BCL3 array and there is a minor difference by means of available power values.

Table 9 Parallel arrays: Power values for different blockage ratios at optimum wake velocity coefficients

Location	Blockage	Opt. α_4	$P_{available}$ (MW)	$P_{extracted}$ (MW)	Power per Swept Area (kW/m^2)
BCL1	0.1	0.35	13.3	21.4	0.314
	0.3	0.35	61.4	115.7	0.483
	0.5	0.40	163.7	315.7	0.773
BCL2	0.1	0.35	14	22.6	0.339
	0.3	0.35	64.8	122.3	0.523
	0.5	0.40	176.2	343.1	0.853
BCL3	0.1	0.35	18	29.1	0.477
	0.3	0.36	83.9	156.1	0.741
	0.5	0.40	233.9	456.9	1.240
BCL0	0.1	0.35	17.1	27.6	0.424
	0.3	0.35	80.9	152.8	0.669
	0.5	0.38	232.2	471.7	1.152
BCL4	0.1	0.35	16.4	26.4	0.417
	0.3	0.35	77.1	145.5	0.654
	0.5	0.38	220.1	443.5	1.120
BCL5	0.1	0.37	10.4	16.3	0.264
	0.3	0.35	49.8	94	0.421
	0.5	0.38	142.3	288.8	0.721

However, once the arrays are deployed further in the west towards Swansea Bay or in the east towards the Severn Estuary, the available power values decrease significantly. From this result, it is possible to deduce that BCL3, BCL0 and BCL4 arrays may be located in a region, which tunes the resonance effect observed in the Channel. This

conclusion should be investigated further using a one-dimensional model of the Channel. However, within the scope of this work, it is not intended to look into the resonance effect of the Channel and how it affects the available power.

Another interesting result from the parametric study is that the available power increases significantly with increasing blockage ratios. For instance, if we consider BCL0 array, the maximum available power is 17.1 MW for a blockage ratio of 0.1. Increasing the blockage by a factor of 3 on the other hand, results in an increase of 4.7 times that of 17.1 MW. A similar trend is observed for each test case considered herein.

The power per turbine swept area parameter also shows that BCL3 is the best performing array. The average water depth within the area of the arrays is not changing considerably. Thus, the change in value of the power per swept area is mainly due to the distance of the array towards the head of the Channel, which affects the resonance of the Channel.

b. Array Connectivity

This section discusses the effects of connecting arrays in series or in parallel on the power availability. For brevity, this section considers three array locations, which were studied in the previous section. Considering BCL3, BCL0 and BCL4, in order to investigate the effects of parallel connectivity, these arrays are divided into two categories. Sub-arrays closer to the English coasts are considered to be located in Region 1 (R1-). Arrays located closer to the Welsh coasts are called Region 2 (R2-). Figure 22 shows the new array locations. Each sub-array is approximately 7 km in length. The distance between arrays is 2.5 km in east-west direction.

In order to compare the maximum available power extracted from the possible combinations, it is important to calculate the power values for the individual arrays. Table 10 summarises the maximum $P_{available}$ for the separate arrays obtained for the optimum α_4 values.

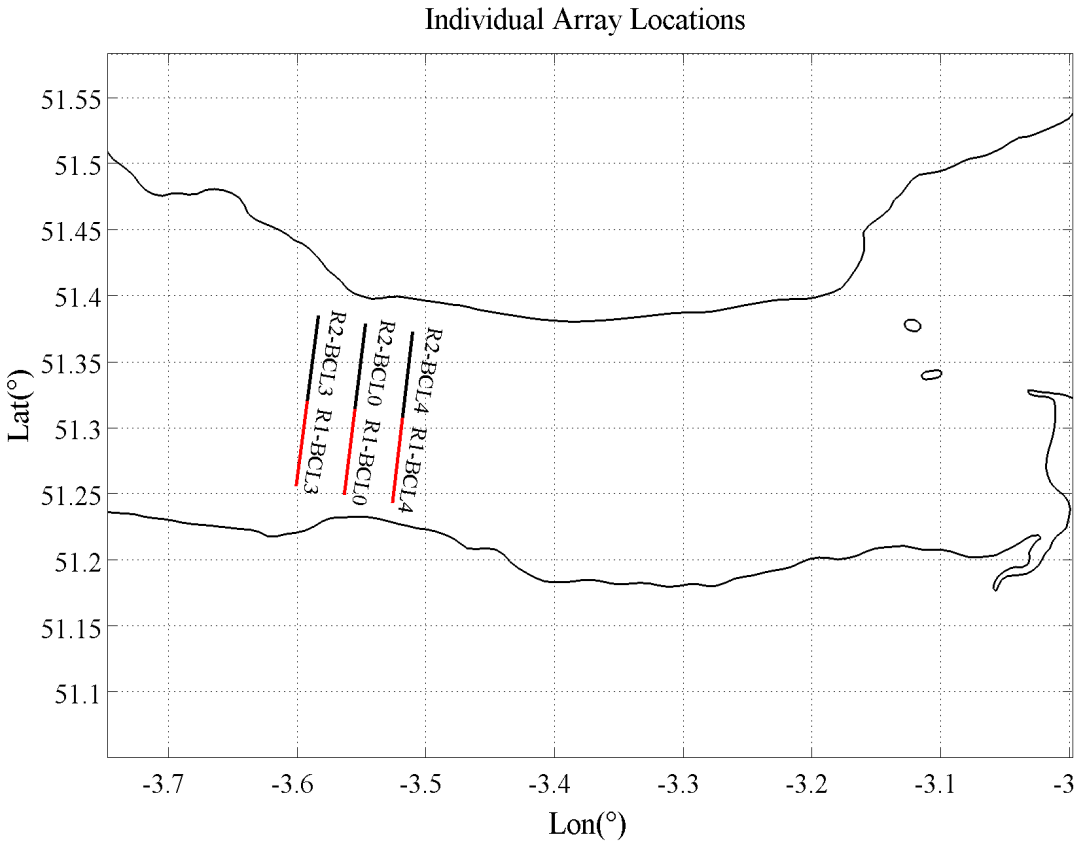

Figure 22 Locations of individual arrays in the Bristol Channel selected for investigating the effects of array connectivity (series and parallel).

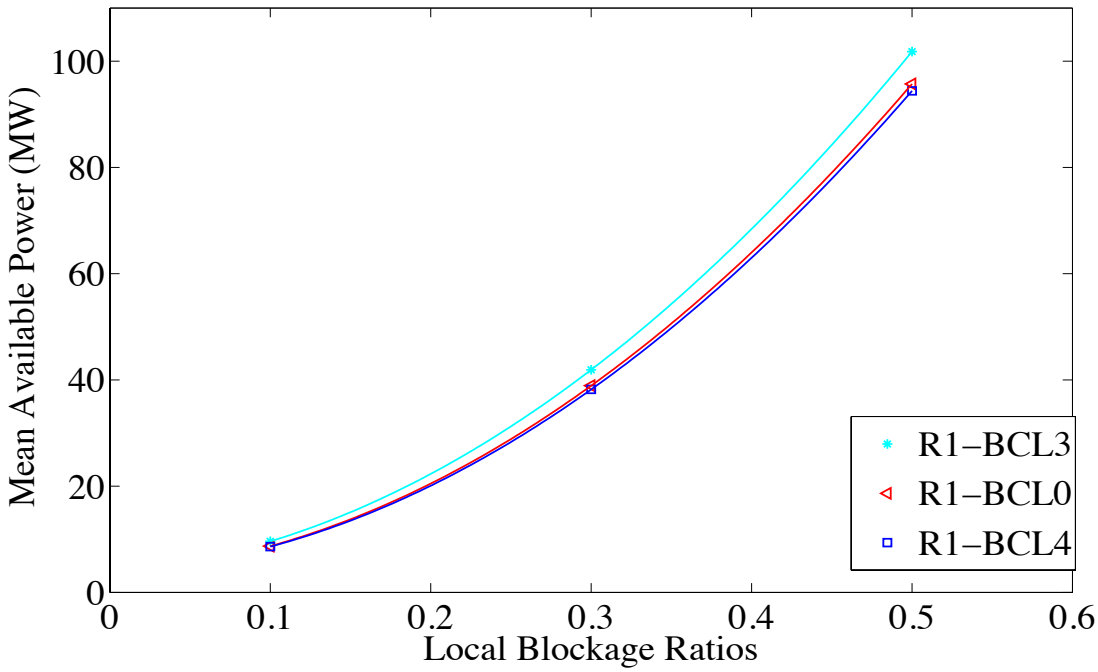

Figure 23 Maximum available power as a function of blockage ratio for the arrays located in Region 1.

The maximum available power values do not change significantly between the two regions, although arrays located in Region 1 (Figure 23) perform slightly better than arrays in Region 2 (Figure 24).

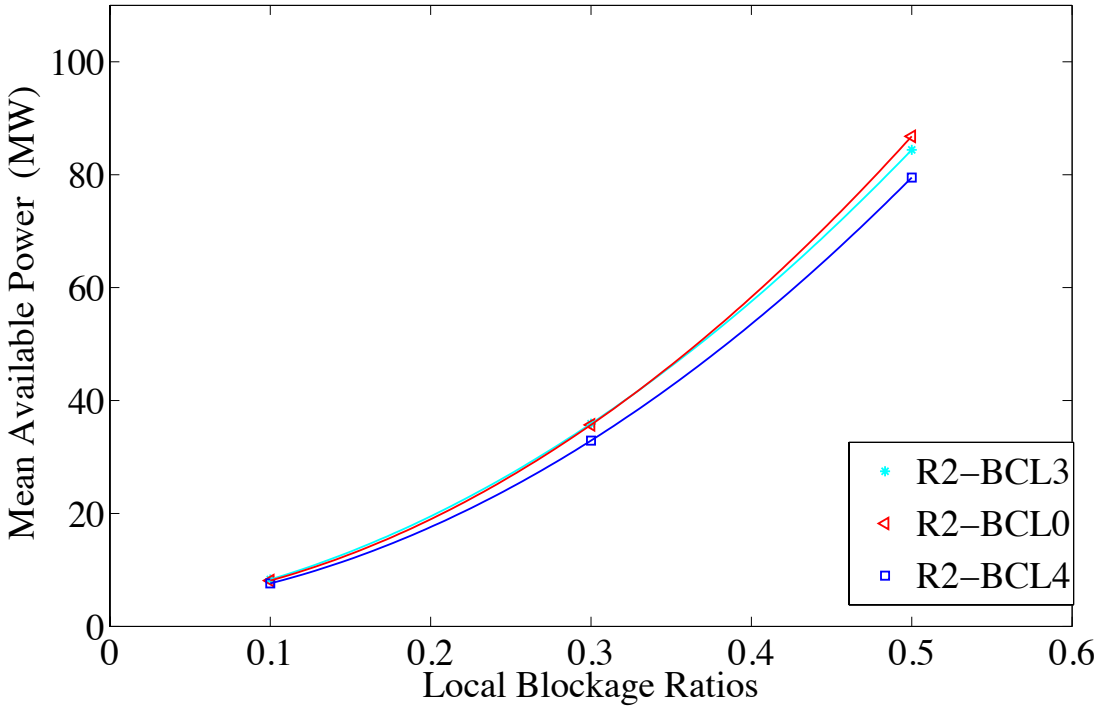

Figure 24 Maximum available power as a function of blockage ratio for the arrays located in Region 2.

Where the power per swept area parameter is concerned, more power is generated per unit area in Region 2 because the turbines located in the Region 1 are smaller than the ones in Region 2. The only exception occurs for R1-BCL4 and R2-BCL4 arrays. If a fixed blockage ratio is applied on R1-BCL4 and R2-BCL4, as the turbine areas in both regions are approximately the same, the power per swept turbine area will vary proportionally with the available power value. In this case, the R1-BCL4 array will always perform better than the R2-BCL4 array. The main reason for this observed difference between the two arrays is the accelerated flow occurring towards the south end of the R1-BCL4 array. The wetting and drying boundary of the English coast is closer to the array location, which enhances the velocities occurring over that region.

Table 10 Maximum available power extracted from individual array configurations. Power per swept turbine area is also given for each blockage ratio

Location	Blockage	Opt. α_4	Average Depth (m)	$P_{available}$ (MW)	Power per Swept Area (kW/m^2)
R1-BCL3	0.1	0.35	28.4	9.6	0.469
	0.3	0.37		41.9	0.683
	0.5	0.44		101.8	0.996
R2-BCL3	0.1	0.35	24.1	8.3	0.478
	0.3	0.37		35.9	0.690
	0.5	0.45		84.4	0.973
R1-BCL0	0.1	0.35	29.9	8.7	0.404
	0.3	0.37		38.9	0.602
	0.5	0.42		95.7	0.889
R2-BCL0	0.1	0.35	26.8	8.1	0.420
	0.3	0.37		35.7	0.617
	0.5	0.43		86.8	0.900
R1-BCL4	0.1	0.35	27.8	8.6	0.430
	0.3	0.37		38.2	0.636
	0.5	0.43		94.4	0.943
R2-BCL4	0.1	0.35	27.0	7.6	0.391
	0.3	0.37		32.9	0.564
	0.5	0.44		79.5	0.818

Parallel Configuration

This subsection discusses the performance of arrays when deployed in parallel. Table 11 shows a brief comparison for BCL3, BCL0 and BCL4 arrays, which correspond to the parallel configuration of arrays installed in isolation. From the table, it is evident that extending the length of an array (as in parallel configuration), the power gain is increased with increasing blockage ratio. For the high blockage case (B=0.5), it is seen that the available power output is increased by 25% for Location 3, 27% for Location 0 (base test) and 34% for Location 4. The placement of the arrays is an important factor in influencing the resonance effect in the Channel. The arrays located in Location 4 (L4) are performing worse compared to the other arrays, as the resonance effect is not emphasised on the distance between L4 and the Atlantic boundary. In this case, it is better to encourage parallel configurations, and extend the length of an array. Figure 25 depicts the power per swept turbine area values for

individual and parallel arrays. It is evident that connecting the arrays in parallel is advantageous.

Table 11 Comparison between arithmetic sums of arrays deployed in isolation and connecting them in parallel for different blockage ratios

Combination	*Blockage*	$\sum P_{available}$ (MW)	*Parallel Array*	*Blockage*	$P_{available}$ (MW)	*Economic Gain*
R1-BCL3	0.1	17.9		0.1	18	1.006
+	0.3	77.8	BCL3	0.3	83.9	1.078
R2-BCL3	0.5	186.2		0.5	233.9	1.256
R1-BCL0	0.1	16.8		0.1	17.1	1.018
+	0.3	74.6	BCL0	0.3	80.9	1.084
R2-BCL0	0.5	182.5		0.5	232.2	1.272
R1-BCL4	0.1	16.2		0.1	16.4	1.012
+	0.3	71.1	BCL4	0.3	77.1	1.084
R2-BCL4	0.5	163.9		0.5	220.1	1.343

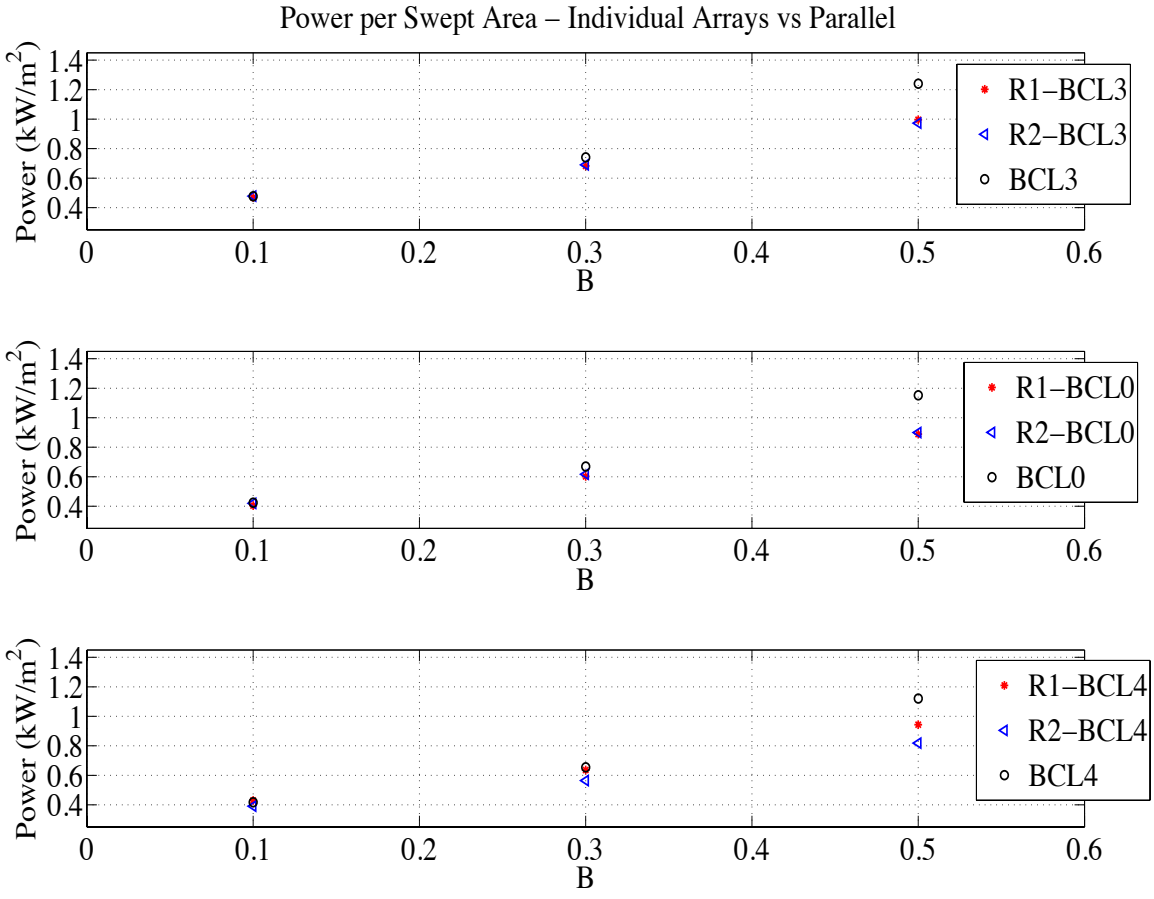

Figure 25 Power per swept area for individual arrays and their parallel configurations

Series Configuration

For arrays connected in series, the maximum available power is reduced. The economic gain factor indicates that a loss in the maximum available power compared to the arithmetic sum of the power values of arrays installed in isolation. However, deployment of the arrays further apart from each other results in a slight recovery in available power. An example of this behaviour is given by R1-BCL30 (series combination of R1-BCL3 and R1-BCL0) and R1-BCL34 (series combination of R1-BCL3 and R1-BCL4) array configurations. For R1-BCL30, the distance between the arrays is 2.5 km and the maximum available power is 161.7 MW for a blockage ratio of 0.5 (see Table 12). As the distance between the arrays is doubled as in R1-BCL34 array configuration, there is a 10.7 MW increment in the available power. The wake recovery downstream of the first array has a positive influence on the power available to the second array.

Table 12 Serial arrays: Power values for different blockage ratios at optimum wake velocity coefficients

Location	*Blockage*	*Opt.* α_4	$P_{available}$ (MW)	$\sum P_{available}$ (MW)	*Economic Gain*
R1-BCL30	0.1	0.35	18	18.3	0.984
	0.3	0.39	74.2	80.8	0.918
	0.5	0.47	161.7	197.5	0.818
R1-BCL34	0.1	0.35	17.9	18.2	0.984
	0.3	0.38	75.9	80.1	0.948
	0.5	0.46	172.4	196.2	0.879
R1-BCL304	0.1	0.36	26	26.9	0.967
	0.3	0.40	103.4	119	0.869
	0.5	0.50	214.1	291.9	0.734
R2-BCL30	0.1	0.36	16	16.4	0.976
	0.3	0.39	64.6	71.6	0.903
	0.5	0.49	135.8	171.2	0.793
R2-BCL34	0.1	0.35	15.6	15.9	0.981
	0.3	0.39	64.8	68.8	0.941
	0.5	0.48	141.6	163.9	0.864
R2-BCL304	0.1	0.35	23.1	24	0.963
	0.3	0.41	89.1	104.5	0.853
	0.5	0.52	176.1	250.7	0.702

When high thrust is applied to the flow, the optimum α_4 values increase in order to compensate possible flow diversion. These findings are coherent with the Anglesey Skerries analysis.

Hydrodynamic Effects

The change in the local hydrodynamics of the Bristol Channel system will be discussed in this section. The analysis conducted herein coincides with the analysis presented in the Anglesey Skerries section.

Figure 26 shows the naturally occurring flow in the Bristol Channel area during an ebb tide. The flow is almost rectilinear, flowing towards the head of the Channel during a flood tide, and out again in ebb tide.

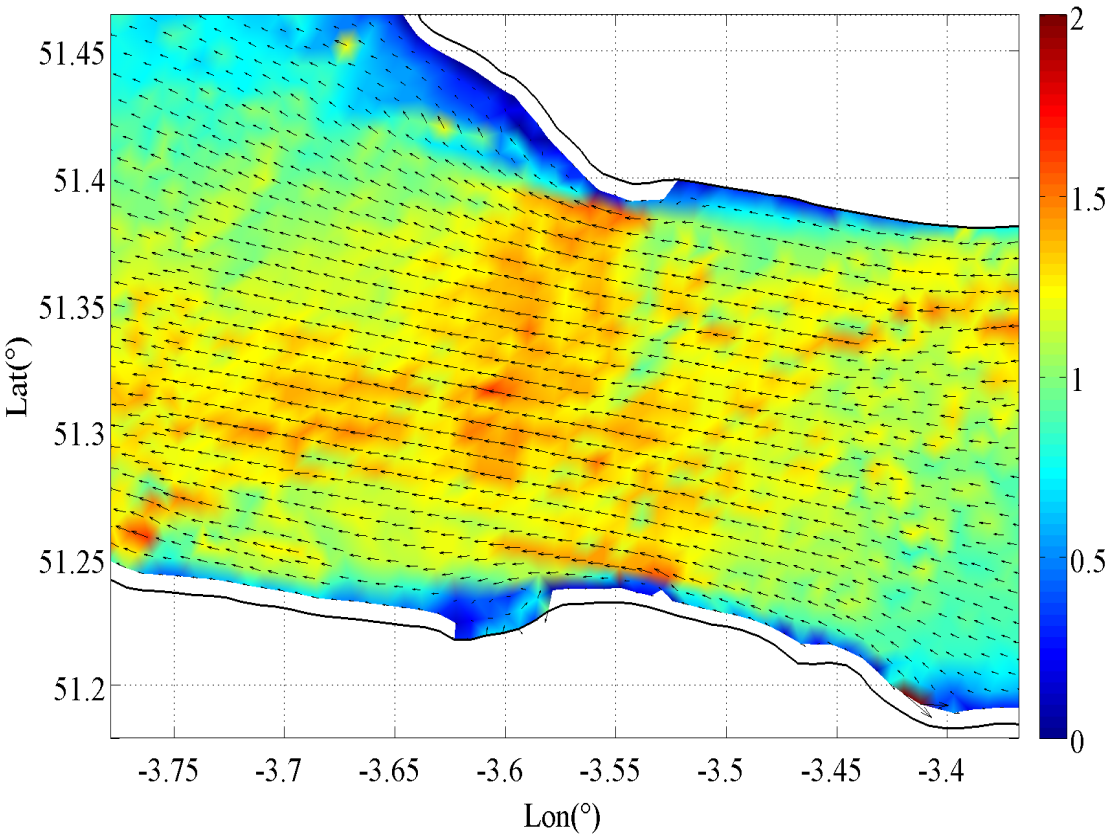

Figure 26 Natural velocity flow field of the Bristol Channel. The vectors are superimposed on the contour plot.

Installation of tidal turbine devices will inevitably alter the flow field. For example, Figure 27 shows the velocity contour plot of an ebb tide for the series configuration of R1-BCL3, R1-BCL0 and R1-BCL4 arrays, with a blockage ratio of 0.5 and wake velocity coefficient of 0.35. From the figure, it is evident that the flow velocity accelerates around the edges of the turbine arrays, causing the flow to divert. The bypass flow speed increases by approximately 1 m/s, whereas the flow passing the turbine arrays slows down as expected.

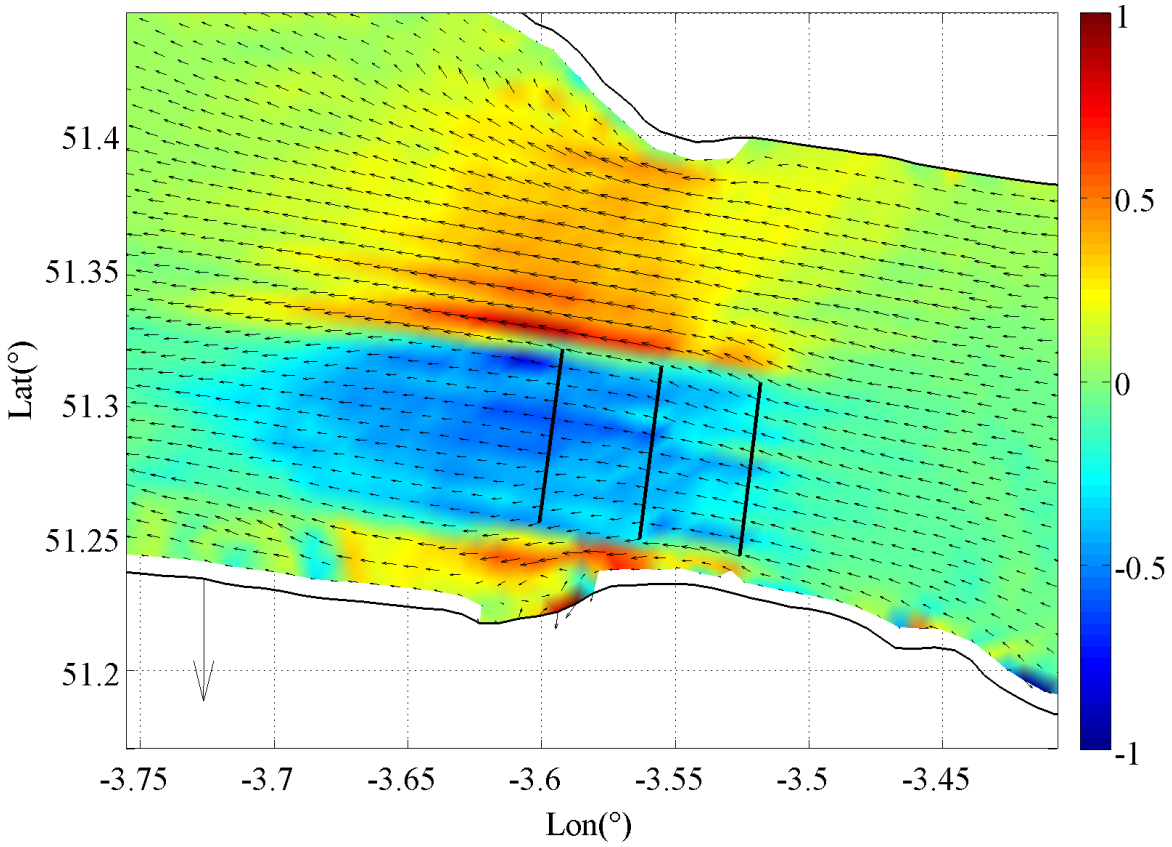

Figure 27 Change in the velocity flow field when R1-BCL3, R1-BCL0 and R1-BCL4 arrays are installed in the Bristol Channel. The vectors are superimposed on the contour plot.

The flow velocity vectors around the wetted areas alter sharply due to the moving boundary treatment in the model. The flow diversion observed in this test case also indicates that the available power is restricted with respect to the thrust applied on the flow.

The flow disturbance is quantified by conducting a harmonic analysis of the velocity data. For brevity, we focus on only BCL0 parallel array configuration for a high blockage test case (B=0.5). The test considers a wake velocity coefficient of 0.35. The quantification of change is computed by focusing on M_2 tidal constituent. It is seen that the amplitude decreases throughout the Channel. The M_2 amplitude decreases approximately 10 cm downstream of the array (towards the head of the Channel), whereas on the upstream, it is around 5 cm.

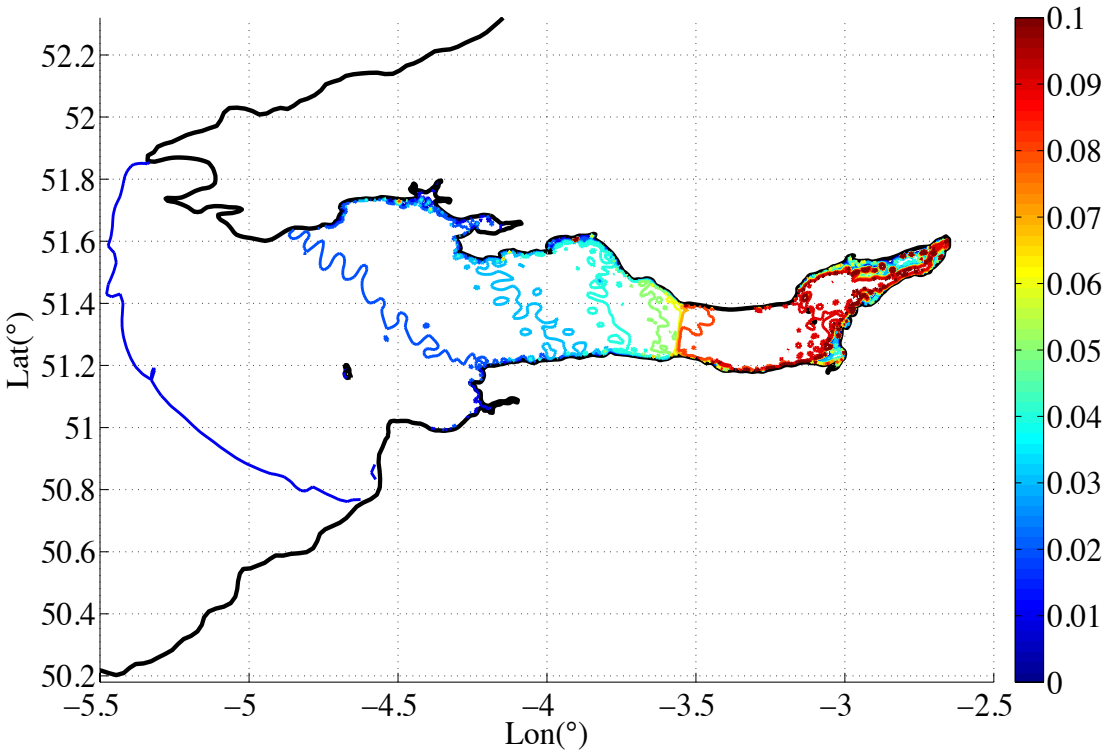

Figure 28 Change in the M_2 amplitude for BCL0 array configuration for B = 0.5 and $\alpha_4 = 0.35$.

Even for a highly blocked case, it is seen that the local hydrodynamics do not alter significantly.

Considering the times of high water (phases), it is observed there is a delay of 6 min (~ 3°) in the area downstream of the deployed array. However, there is no change observed on the upstream of the array (see Figure 29).

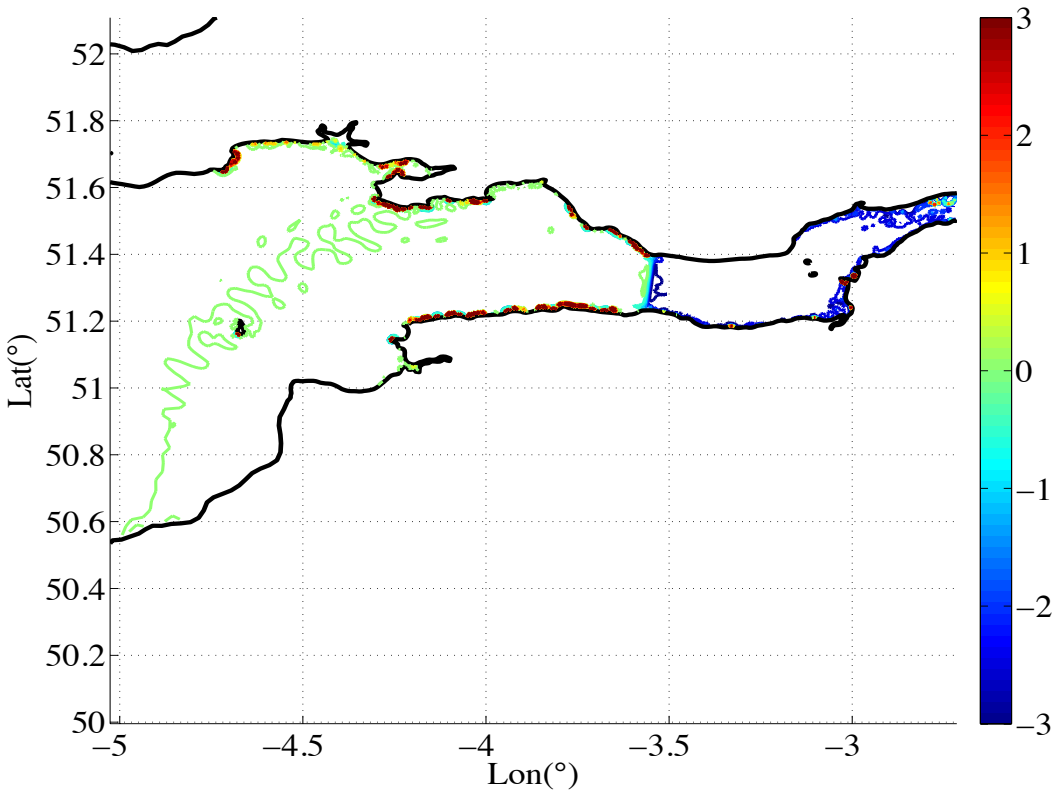

Figure 29 Change in the M_2 phases using BCL0 array configuration when B=0.5 and α_4 = 0.35. Blue contour line indicates a 3° difference between natural and altered flow M_2 phases. Green contour line shows no change (0°).

4. Pentland Firth

Much of the analysis of the Pentland Firth has been written up as technical papers for peer reviewed journals. At time of writing one of these has been accepted and three others are currently under review. The accepted paper, analysing the maximum available power from the Pentland Firth, is included as an appendix to this report.

Tidal Hydrodynamics

In the natural state (i.e. without any tidal devices) the current in the Pentland Firth lags the head difference across the straight caused by the difference in water level. This lag varies over the spring/neap tidal cycle. We determine the phase difference by calculating the instantaneous phase from the analytic signal of the head difference at the time when the current is at a maximum. The phase lag calculated from our model varies between 33° at spring tide to 52° at neaps. In the terminology of Garrett & Cummins (2005), the Pentland Firth is therefore somewhere between a drag dominated tidal channel (where current and elevation difference are in phase) and an

inertia dominated channel (where they are 90° out of phase). However, the channel is significantly closer to an inertia-dominated channel at neap tide than at spring tide.

The integrated flow through the Pentland Firth is not perfectly symmetric over the tidal cycle, with slightly stronger flows on the flood tide (current flowing west to east) and weaker flows on ebb tides. The current is largest in the shallow areas around the islands (Swona and Stroma) and close to the headlands (e.g. Duncansby Head) where tidal races exist. The currents are also large enough for tidal stream energy devices at several transects across the whole channel.

Power Analysis

In this study we consider turbine rows at the locations shown in Figure 30. The rows of turbines are included as in the previous section as line discontinuities with the implementation described in WG3WP6D5 and in Serhadlıoğlu *et al.* (2013). In this study we considered three different blockage ratios: B=0.1; B=0.25; B=0.4. This allows us to examine the dependence of available power on blockage.

In this section, all results are presented for a model, which is run for 9 days. This allows 1.5 days for spin up and then allows us to analyse the variation in power over the spring/neap tidal cycle. The model is forced with M_2 and S_2 tidal components.

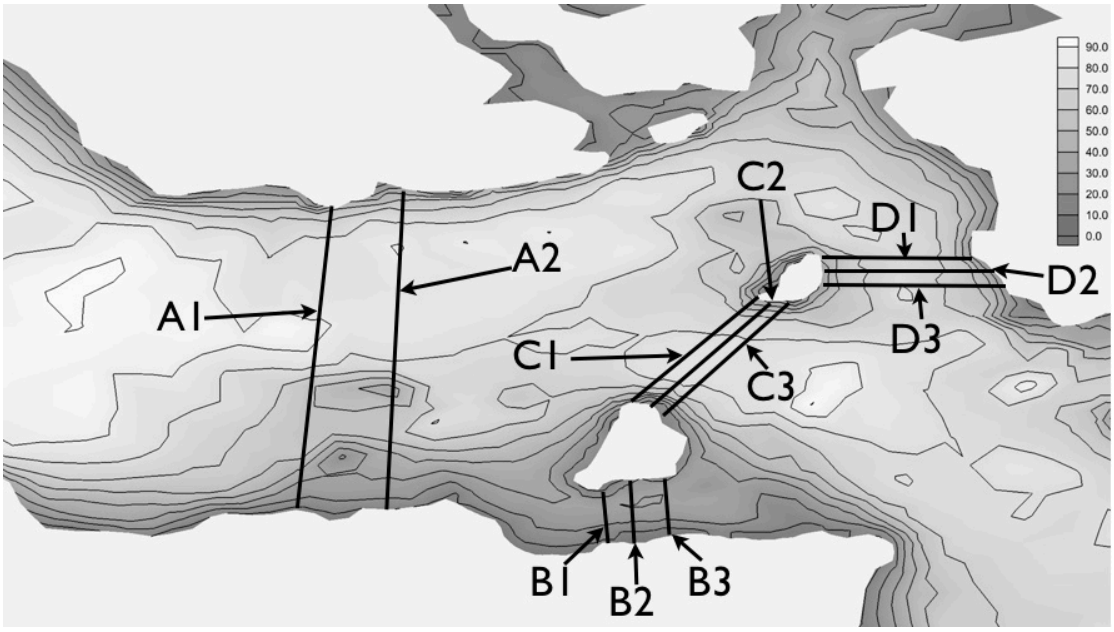

Figure 30 Locations of turbines used in study of Pentland Firth. Water depths are shown by contours.

As described in the previous section it is necessary to run the model for a variety of wake induction factors. In our study of the Pentland Firth we accounted for the small variation in the optimum wake induction factor over the spring/neap tidal cycle as described in the next paragraph. However, the extra power obtained from varying the wake induction factor is negligible and so it was decided not to undertake this in our studies of Anglesey and the Bristol Channel.

To obtain the optimum available power, model simulations were therefore undertaken for a variety of wake velocity coefficients and the time-varying available power computed in each case in order to interpolate a time-varying optimum wake velocity coefficient. More specifically, for each value of wake velocity coefficient, the time-varying available power was low-pass filtered, so as to average the result over approximately an M_2 tidal period. Every minute, the optimum filtered available power and wake velocity coefficient were then interpolated (using a spline) from the available power estimates obtained for each of the wake velocity coefficients. (This approach assumed that changes in the wake velocity coefficient over the spring–neap cycle are sufficiently small and gradual that only the magnitude of the coefficient, and not its variation, affects the tidal dynamics within the Pentland Firth at any given

time.) Finally, the maximum time-averaged available power owing to M_2 and S_2 tides was calculated by taking the average over half of the spring–neap cycle.

To illustrate the methodology used to analyse the data, consider the case where there are three rows of turbines at B1, B2, B3, C1, C2, C3 and D1, D2, D3 with B=0.4. Simulations have been undertaken for α_4 =0.35, 0.45, 0.55 and 0.65. Figure 31a shows the raw available power output for α_4 =0.35. Figure 31b presents the available power in the first half of the spring–neap cycle after low-pass filtering, for each value of wake velocity coefficient, as a function of time. Figure 31c shows splines fitted to the available power for varying α_4 at the extremes of spring tide and neap tide. The wake velocity coefficient that maximizes the available power through the spring–neap cycle is shown in Figure 31d.

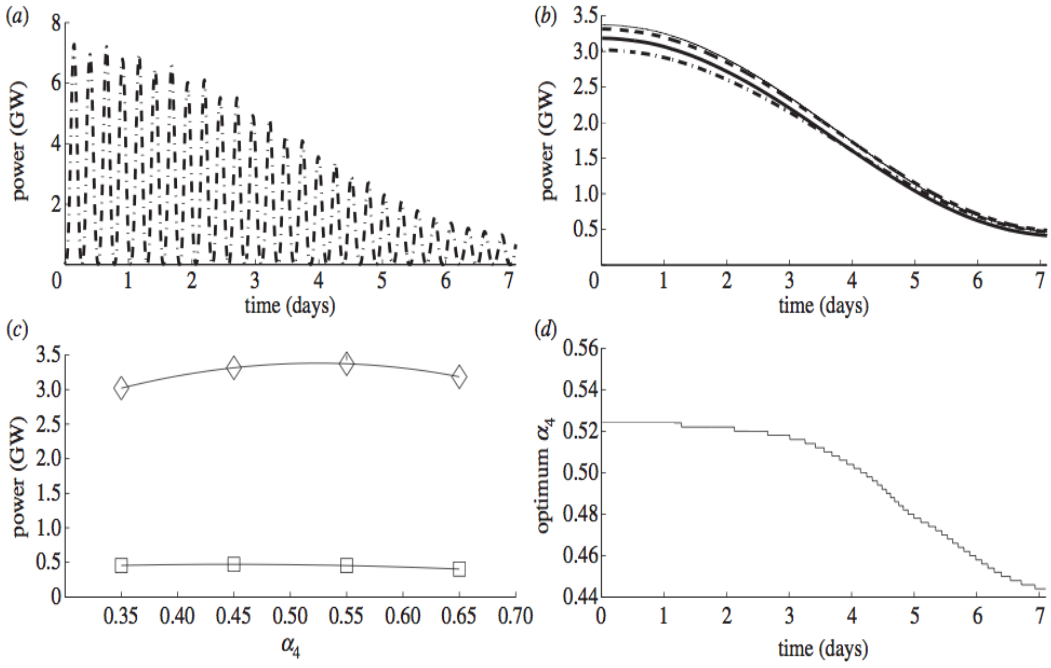

Figure 31 Example analysis over the tidal cycle. (a) Raw available power for α_4=0.35; (b) low-pass filtered power for α_4=0.35 (dashed-dotted line), α_4=0.45 (dashed line), α_4=0.55 (thin line), α_4=0.65 (thick line); (c) available power at spring (diamonds) and neap (squares) tide and spline fit, and (d) optimum α_4 over tidal cycle.

A deployment parameter study has been undertaken concerning the available power when up to five rows of turbines extended across the entire Pentland Firth. Deployments with a single row of turbines are located at B1, C1 and D1 (figure 4). Deployments comprising two rows of turbines are considered at B1, B2, C1, C2, D1 and D2. Deployments of three rows of turbines are investigated at B1, B2, B3, C1, C2, C3, D1, D2 and D3. When four or five rows are considered, the turbines are placed at the same locations as for the three rows, and also at A1, and A1 and A2. In all cases, the maximum time-averaged available power quoted is the average value given by the analysis technique described in above. Table 13 summarises the resulting power estimates, from which it is obvious that the power available for generation increases as additional rows of turbines are added. There is also greater available power, for a given number of rows, when a larger blockage ratio is used. However, there is a diminishing return as additional rows are deployed—two rows of turbines produce less than twice the power of one row of the same turbines Vennell (2012).

As with the other sites there is a clear hydrodynamic benefit to making to having a large local blockage — i.e. making the turbines are large as possible and reducing the spacing between them. Further it is clearly advantageous in terms of maximizing the available power to have a small number of rows with high blockage rather than many rows with a lower blockage.

Table 13 Average available power from Pentland Firth for different array configurations

Turbine rows	Blockage	Time-averaged power (GW)
B1, C1, D1	0.4	1.01
B1, B2, C1, C2, D1, D2	0.4	1.58
B1, B2, B3, C1, C2, C3, D1, D2, D3	0.4	1.94
A1, B1, B2, B3, C1, C2, C3, D1, D2, D3	0.4	2.16
B1, B2, B3	0.4	0.10
C1, C2, C3, D1, D2, D3	0.4	1.76
B1, C1, D1	0.25	0.52
B1, B2, C1, C2, D1, D2	0.25	0.91
B1, B2, B3, C1, C2, C3, D1, D2, D3	0.25	1.20
A1, B1, B2, B3, C1, C2, C3, D1, D2, D3	0.25	1.49
B1, C1, D1	0.1	0.17
B1, B2, C1, C2, D1, D2	0.1	0.33
B1, B2, B3, C1, C2, C3, D1, D2, D3	0.1	0.47
A1, B1, B2, B3, C1, C2, C3, D1, D2, D3	0.1	0.56
A1, A2, B1, B2, B3, C1, C2, C3, D1, D2, D3	0.1	0.63
B1	0.1	0.011
C1, D1	0.1	0.159

It may be desirable not to place turbines across the entire channel width of the Pentland Firth in order to leave shipping lanes free, or because of a preference to develop the site in stages so that only certain locations are blocked at a particular time.

Because one of the first areas of the Pentland Firth, which is likely to be developed, is the Inner Sound (location B), we choose to investigate the likely interaction between this subchannel and those to the North of Swona. Table 13 summarizes the time-averaged available power predicted by the numerical model when turbines are deployed across B and not across C and D, or across C and D but not B. From Table

13, it is clear that when a single row of low blockage turbines (i.e. B =0.1) is deployed in the Pentland Firth the sum of the power available when turbines are placed solely at B, or at C and D, is nearly identical to the total power available when turbines are simultaneously deployed across all rows. This is simply because a single row at each location leads to minimal disruption to the flow. For three rows of turbines with a much higher blockage of B =0.4, there is a larger reduction in the available power (approx. 4%) when turbines are not deployed across all rows simultaneously; however, this result is of relatively low magnitude. It therefore appears, for a feasible number of turbines, that interaction effects in the Inner Sound will be small. Interaction effects will be slightly more significant at other locations, such as the subchannel between Swona and Stroma, provided turbines can be installed there.

Hydrodynamic Effects

Placing a large deployment of tidal turbines in the Pentland Firth will cause changes to the naturally occurring tidal hydrodynamics. Figure 32 shows the change to the M_2 water levels across the entire computational domain between the naturally occurring case and the case with three rows of turbines. It can be seen that the disturbance is confined to the Pentland Firth itself and Scapa Flow. Outside this area the change in water level is less than 4 cm.

Although the water levels outside the Pentland Firth remain nearly unchanged the hydrodynamics within the channel will change. The M_2 water level amplitude within the strait when three rows of turbines are deployed is shown in Figure 33. To examine the changes to the current within the Pentland we consider the point 58°43’01’’N, 003°05’09’’W which is in the centre of the Pentland Firth between Stroma and Swona. In Figure 34, we consider consider the change to the maximum current observed at this point for different levels of power extraction. It can be seen that to extract a substantial amount of power requires a significant change to the flow through the Pentland Firth.

Figure 32 Difference in M_2 water level between natural case and a case with 3 rows of turbines

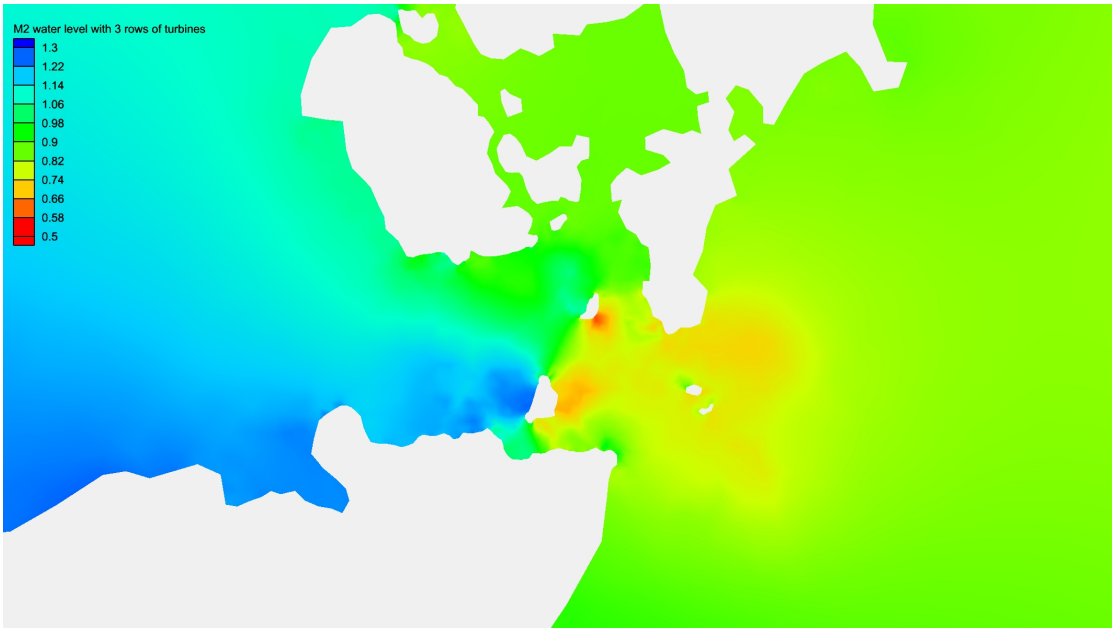

Figure 33 M_2 water level in the Pentland Firth with 3 rows of turbines

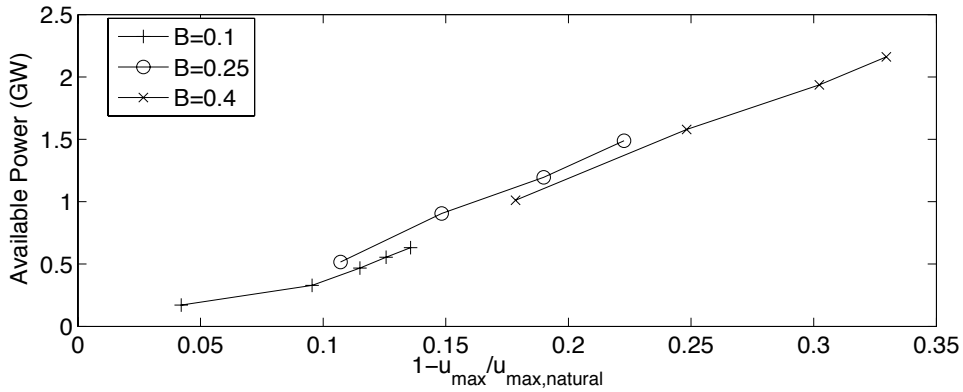

Figure 34 Change to the current in the Pentland Firth at peak energy extraction

5. Conclusions

In this report we have modelled the inclusion of tidal turbines at a headland site (Anglesey), an estuary site (Bristol Channel), and a strait (Pentland Firth). Similar methodologies have been successfully applied to the various different sites. The available power has been analysed at all sites and the hydrodynamic effect of including turbines analysed. It is found that when significant power is extracted there is a substantial change to the current at a site, but that the hydrodynamic changes are confined to vicinity of the site.

REFERENCES

Adcock T.A.A., Draper S., Houlsby G.T. and Borthwick A.G.L., On the tidal resource of the Pentland Firth, 4th International Conference on Ocean Energy, Dublin, Ireland, 2012.

Adcock T.A.A., Draper S., Houlsby G.T., Borthwick A.G.L., and Serhadlıoğlu, S., The available power from tidal stream turbines in the Pentland Firth, *Proc. R. Soc. Lond. A*, vol. 469, 2013.

Admiralty Tide Tables Vol.1, United Kingdom and Ireland, Including European Channel Ports, 1997.

Bunya S., Kubatko E.J., Westerink J.J., and Dawson C.A., A wetting and drying treatment for the Runge-Kutta discontinuous Galerkin solution to the shallow water equations, *Compt. Methods Appl. Mech. Engineering*, vol. 198, pp.1548-1562, 2009.

Black and Veatch Ltd. Phase II: UK tidal stream energy assessment, Technical Report, 2005.

Blunden L.S., and Bahaj A.S., Initial evaluation of tidal stream energy resources at the Portland Bill, UK, *Renew. Energy*, vol. 31, pp: 121-132, 2006.

Draper S., Tidal stream energy extraction in coastal basins, DPhil Thesis, University of Oxford, 2011.

Draper S., Borthwick A.G.L., and Houlsby G.T., Energy potential of a tidal fence deployed near a coastal headland, 9th EWTEC, Southampton, UK, 2011.

Falconer, R. A., An introduction to nearly-horizontal flows, *Coastal, Estuarial and Harbour Engineer's Reference Book*, Chapman & Hall, 1993.

Fong, S. W., and Heaps, N. S., Note on quarter-wave tidal resonance in the Bristol Channel, Institute of Oceanographic Sciences, Report No. 63, 1978.

Houlsby G.T., Draper S., Oldfield, M.L.G. Application of Linear Momentum Actuator Disc Theory to open channel flow, Technical report, Department of Engineering Science, University of Oxford, January 2008.

Howarth M.J., Currents in the eastern Irish Sea, Oceanography and Marine Biology, An Annual Review, vol. 22, pp. 2-47, Aberdeen University Press, 1984.

Godin G., On the predictability of currents, International Hydrographic Review, Monaco, LX (1), 1983.

Kubatko E.J., Westerink J.J., and Dawson C., hp discontinuous Galerkin methods for advection dominated problems in shallow water flow, *Comput. Methods Appl. Mech. Engrg*., vol. 196, pp. 437-451, 2006.

Nadaoka K., and Yagi H., Shallow-water turbulence modelling and horizontal large-eddy computation of river flow, J. Hydraul. Eng., vol. 124, pp. 493-500, 1998.

Nishino T. and Willden R. H. J., The efficiency of an array of tidal turbines partially blocking a wide channel, *Journal of Fluid Mechanics*, vol. 708, pp. 596-606, 2012.

Owen A., The tidal regime of the Bristol Channel: a numerical modelling approach, *Geophys. J. R. ast. Soc*., vol. 62, pp: 59-75, 1980.

Pugh D.T., *Tides, surges and mean sea-level*, John Wiley & Sons, Chichester, 1987.

Serhadlıoğlu S., Houlsby G.T., Adcock T.A.A., Draper, S. and Borthwick A.G.L., Assessment of tidal stream energy resources in the UK using a discontinuous Galerkin finite element scheme, 17th International Conference on Finite Elements in Flow Problems, San Diego, California, 2013.

Stansby P.K., Limitations of depth-averaged modelling for shallow wakes, *Journal of Hydraulic Engineering*, vol. 132, pp: 737-740, 2006.

Stansby P., and Lloyd P. M., Wake formation around islands in oscillatory laminar shallow-water flows. Part. 2. Three-dimensional boundary-layer modelling, *Journal of Fluid Mechanics*, vol. 429, pp. 239-254, 2001.

Taylor G. I., Tides in the Bristol Channel, *Proc. Camb. Phil. Soc*., vol. 20, pp: 320-325, 1921.

U.K. Government Department of Energy and Climate Change, Severn Tidal Power Feasibility Study: Conclusions and Summary Report, October 2010.

Uncles R.J., A numerical simulation of the vertical and horizontal M_2 tide in the Bristol Channel and comparisons with observed data, *Limnol. Oceanogr*. vol. 26, No. 3, pp: 571-577, 1981.

Uncles R. J., Hydrodynamics of the Bristol Channel, *Marine Pollution Bulletin*, vol. 15, No. 2, pp: 47-53, 1983.

Vennell R., Tuning tidal turbines in-concert to maximize farm efficiency, *Journal of fluid mechanics*, vol. 671, pp. 587-604, 2011.

Vogel C. R., Willden R. H. J., and Houlsby G. T., A correction for depth-averaged simulations of tidal turbine arrays, 2013a, 10th EWTEC, Aalborg, Denmark, Submitted.

Vogel C. R., Houlsby, G. T., and Willden R. H. J., On the extractable power of an array of turbines partially spanning a wide channel with a free surface, *Journal of Fluid Mechanics*, 2013b, Submitted.